Approximating Fluid Bearing Characteristics using Polynomials for the Nonlinear Dynamics of Rotating Machines

T.A. El-Sayed[a,b,c,*], Michael I. Friswell[d], Hussein Sayed[a,e]

[a]*Department of Mechanical Design, Faculty of Engineering, Mataria, Helwan University, P.O. Box 11718, Helmeiat-Elzaton, Cairo, Egypt*
[b]*Centre for Applied Dynamics Research, School of Engineering, University of Aberdeen, Aberdeen, AB24 3UE, UK*
[c]*School of Engineering, University of Hertfordshire Hosted by Global Academic Foundation, Cairo, Egypt*
[d]*Faculty of Science and Engineering, Swansea University, Bay Campus, Fabian Way, Crymlyn Burrows, Swansea SA1 8EN, UK*
[e]*High Institute for Engineering & Technology Al-Obour (Km 21 Cairo-Belbeis Road-Obour City), Egypt*

Abstract

Modelling the nonlinear dynamics of rotors supported by finite length journal bearings is of great importance in various engineering applications. In this study, four-dimensional polynomial functions are evaluated to represent the nonlinear hydrodynamic force based on a previously evaluated database. These functions are then used to model the dynamics of flexible rotor/bearing systems. The quasi statics and dynamics of rotor-bearing systems are investigated, and the results are compared with the numerical solution obtained by solving the Reynolds equation at each time step. The findings indicate that the current analysis yields favorable agreement with the direct solution of Reynolds equation in both perturbation analysis from the equilibrium position and dynamic analysis. Moreover, the analysis reveals that the computational time required to solve the dynamics of rotor-bearing systems is significantly lower than that of solving Reynolds equation at each time step to acquire the bearing forces.

Keywords: Rotor-bearing dynamics,four-dimensional polynomial representation, Reynolds' equation, polynomial fitting, finite length journal bearing, Hopf bifurcation analysis, numerical continuation method .

*Corresponding author
Email addresses: tamer.elsayed@abdn.ac.uk (T.A. El-Sayed), m.i.friswell@swansea.ac.uk (Michael I. Friswell), husseinsayed2008@m-eng.helwan.edu.eg (Hussein Sayed)

1. Nomenclature

c	Radial clearance in meters
c_h	Housing damping coefficient in Newton-seconds per meter
$\bar{C}_H$	Dimensionless damping coefficient for bearing housing, $\bar{C}_H = \frac{c_h\ \Omega\ c}{W}$
e	Eccentricity between the bearing and journal centers in meters
e_u	Eccentricity of the unbalance mass in meters
$F_x,\ F_y$	Journal bearing forces in the directions of x and y respectively, in Newtons
$\bar{F}_X,\ \bar{F}_Y$	The dimensionless components of bearing forces $\bar{F}_X = \frac{F_x}{W} = \frac{F_X}{W},\ \bar{F}_Y = \frac{F_y}{W} = \frac{F_Y}{W}$
$\bar{F}_U$	Dimensionless unbalance force amplitude defined as $\bar{F}_U = \frac{m_u\ e_u\ \Omega^2}{W}$
h	Thickness of the oil-film in meters
H	Dimensionless oil-film thickness, $H = \frac{h}{c}$
k_i	Housing and shaft stiffness constants $i = h,\ s$ in Newtons per meter
$\bar{K}_I$	Dimensionless housing and shaft stiffness $\bar{K}_I = \frac{k_i\ c}{W}$
m	Total mass of the rotor $m = m_d + 2m_j$ in kilograms
m_i	Housing mass, disc mass and journal mass, $i = h,\ d,\ j$ in kilograms
m_u	Unbalance mass in kilograms
$\bar{M}$	The dimensionless rotor mass, given by $\bar{M} = \frac{m\ c\ \Omega^2}{W}$
p	The pressure of the lubricating fluid film in Pascals
P	Dimensionless fluid film pressure, given by $P = \frac{p}{6\mu\Omega}\left(\frac{c}{R}\right)^2$
P_n	Normalized dimensionless pressure defined as $P_n = \frac{P}{\sqrt{(X+2Y')^2+(2X'-Y)^2}}$
r	The radius of the rotor in meters
R	The radius of the bearing in meters
S	Sommerfeld number, defined as $S = \frac{\mu\Omega r L}{\pi W}\left(\frac{r}{c}\right)^2$
t	Time in seconds.
W	Static load in Newtons.
$\bar{W}$	Dimensionless static load, defined as $\bar{W} = \frac{L/D}{3\pi\ S}$
x, y	Displacements of the journal center with respect to bearing housing
x_i, y_i	Displacements of housing, disc, and journal centers $i = h,\ d,\ j$ in meters
$X,\ Y,\ X', Y'$	Dimensionless displacements and velocities of the journal center with respect to bearing housing
X_I, Y_I	Dimensionless position of the housing, disc and journal centers $I = H,\ D,\ J$
X_I', Y_I', X_I'', Y_I''	Bearing housing disc and journal centers dimensionless velocities and accelerations respectively, $I = H, D, J$.
z	Axial coordinate in meters
Z	Dimensionless location in axial direction $Z = \frac{z}{R}$
ε	The ratio between the eccentricity and radial clearance $\varepsilon = e/c$
θ	Attitude angle of the journal bearing, expressed in radians
μ	Viscosity of the fluid film in the bearing, measured in Pa·s
ρ	The density of the bearing fluid film in kg per cubic meter
τ	Dimensionless time, defined as $\tau = \Omega t$
ϕ	Circumferential coordinate in radians
Ω	Rotational velocity of the journal, expressed in radians per second

Introduction

Bearing are essential machine components that used to minimize the friction between moving parts and support loads, typically from a rotating shaft. The two broad categories of bearings are

sliding contact bearings and rolling contact bearings. The selection of a specific type depends on the application and design requirements. Rolling contact bearings can be categorized as either spherical bearings or roller bearings, while sliding contact bearings can be classified into journal and thrust bearings. Rolling bearings are commonly utilized in industrial applications due to their low starting friction, smaller axial space requirement, lower maintenance and gradual failure. In contrast, journal bearings are better suited for managing shocks and overloads compared to ball bearing.

In addition, journal bearings operate effectively at relatively high rotational speeds with low levels of noise due to the lubricating fluid film that separates the rotating shaft and the journal bearing, see for example, [1]. Another advantage of journal bearings is that the working fluid media may acts as a lubricant, which makes it commonly used in pumps and hydraulic turbochargers for water desalination plants [2, 3]. The scope of this study is on the dynamics of systems that involve journal bearings.

In journal bearings, a radial clearance exists between the journal and the bearing, which is filled with a thin layer of oil or other fluid, depending on the design. The pressure distribution in this layer can be accurately described by a partial differential equation known as Reynolds equation [4]. However, finding an exact solution for this equation is challenging, as shown in previous studies [5]. To simplify the equation, some assumptions are made, and it can be reduced to a form that can be analytically solved. The most common forms after this reduction are the short bearing form, as shown in previous studies [6–9] and the long bearing form, as shown in previous studies [10, 11]. However, for finite length bearings, these simplifications are no longer valid, and numerical methods such as finite difference and finite element methods [12–14], finite volume method [15], perturbation methods [16], and meshless methods [17] are used to solve the Reynolds equation. Moreover, some research has used computational fluid dynamics to model the fluid film between the rotor and the journal bearing and to evaluate the bearing forces.

Accurate modelling the dynamics of a rotor supported by journal bearings requires the evaluation of bearing forces at each timestep. Analytical solutions are available for the bearing forces of both short and long bearings, enabling quick dynamic analysis. However, in the case of finite length bearings or bearings with internal grooves, no analytical solution exists, and numerical methods such as the finite element method (FEM) or finite difference method (FDM) must be used to evaluate bearing forces at each dynamic timestep. This can be computationally expensive and memory-

intensive, particularly when using fine meshes to solve the Reynolds equation. Moreover, if the shaft is supported by unsymmetric bearing arrangements, bearing forces must be evaluated for each bearing at each timestep, increasing the complexity. Hence, finding an accurate and efficient method for evaluating journal bearing forces remains a challenging task, and is the main focus of this study.

The method of representing the journal bearing as equivalent stiffness and damping coefficients is commonly used to simplify the problem for rotor bearing systems. This approach dates back to the mid-twentieth century and is still used today, see studies (e.g., [18–22]). The process of evaluating the bearing coefficients is challenging and requires solving the Reynolds equation, which can be achieved through various techniques such as analytical [23, 24], finite difference [25–27], finite element [28, 29], computational fluid dynamics [30], and experimental methods [31]. Someya, et al. [32] even introduced data tables to simplify the process of evaluating bearing coefficients.

The dynamic analysis of rotor-bearing systems based on these coefficients is appropriate for speeds below the threshold speed, beyond which a Hopf bifurcation occurs. At this point, the linear bearing coefficient solution shows unstable responses that do not agree with experimental findings reported by researchers such as Muszynska [33] and Deepak and Noah [34]. These studies demonstrated that above the threshold speed, stable whirling is observed. As a result, researchers were motivated to develop more accurate models that enable the evaluation of bearing responses at speeds above the threshold.

Efforts to extend the validity of bearing solutions beyond the threshold speed have included evaluating second order bearing coefficients [35–37]. Further analysis based on higher order bearing coefficients was developed, see [24, 38, 39]. It has been found that solutions obtained using second and higher order bearing coefficients have very similar responses to those derived using linear bearing coefficients up to the threshold speed. At this speed, Hopf bifurcation occurs. Beyond the critical speed, the solution does not exhibit divergence but instead manifests as a limit cycle solution. Furthermore, the classification of the Hopf bifurcation as either supercritical or subcritical can be determined. However, this solution has limitations. The bearing coefficients are obtained using perturbation methods and are accurate only in the proximity of the journal static equilibrium point. When the rotor whirls in larger limit cycles, the bearing coefficients become inaccurate for evaluating the bearing forces. In addition, it has been proved that the stiffness and damping equivalent coefficients of a bearing undergo alterations when the applied static load undergoes variations. This

factor restricts the comprehensive dynamic analysis of the system, confining it to specific static loads and necessitating the consideration of multiple coefficients for each load scenario.

There have been numerous attempts to evaluate an approximate analytical methods for assessing the hydrodynamic forces in journal bearings with finite length. As early as 1963, Fedor [40, 41] developed an approximate analytical solution to evaluate the pressure distribution in journal bearing while considering the finiteness of the bearing with incomplete oil film boundary conditions. In 1980, Barrett, et al. [42] introduced a quick approximate method to evaluate the nonlinear response of journal bearing, considering the finiteness of the bearing, by using correction factors based on the analytical solution obtained from the short bearing theory. Hirani, et al. [43] combined the short and long bearing theories to introduce an approximate closed-form pressure distribution for finite-length bearings. Bastani and de Queiroz [44] developed a correction function for the infinitely short bearing model and the infinitely long bearing model to represent the forces of finite-length bearings.

Wang, et al. [45] utilized the principle of variable separation to propose an approximate analytical solution for journal bearings with finite length. They found that their model results agreed well with those from the finite difference method. Zhang, et al. [46] introduced a semi-analytical solution to evaluate the nonlinear fluid film forces of hydrodynamic journal bearings with two axial grooves. Vignolo, et al. [47] used a perturbation analysis to evaluate an approximate analytical solution for Reynolds equation. They proposed that the zero-order analysis is valid for short bearings and the first-order analysis is valid for finite length bearing up to $L/D \in [1/8 - 1/4]$.

Gong, et al. [48] obtained an approximate analytical solution for the pressure distribution in the bearing clearance using a regular perturbation method, and they showed the range of applicability of their results compared with the numerical results. Zhang, et al. [49] introduced a method for evaluating the oil film pressure distribution for finite length journal bearings based on the variational principle. Dyk, et al. [21] used approximate analytical solutions to Reynolds equation to explore the stability of finite-length journal bearings.

In the last two decades, another approach for evaluating bearing forces has gained attention, which involves using a database. This technique has been investigated by several researchers, including Chasalevris, et al. [50], Chen and Tseng [51], and Wang and Khonsari [52]. The method involves generating a database of bearing forces corresponding to various ranges of bearing parameters. The resulting database can be used to quickly and accurately predict the bearing forces using

an interpolation method.

Obtaining a function that accurately fits a large set of response data is a fundamental task in dynamical analysis. Linear or polynomial regressions are commonly used to achieve this goal, where a single dependent variable is considered [53, 54]. However, when the number of dependent variables increases, the problem becomes more complex and is referred to as a multivariate regression problem [55].

Higher-order multivariate polynomial regression has been successfully employed in various applications, such as predicting human affective states from facial, physiological, and central nervous system data [56]. Experimental results have shown that the multivariate polynomial regression method is efficient and can achieve prediction accuracies with RMS error 2%. In another application, Su, et al. [57] utilized multivariate polynomial regression to estimate the compressive strength of ground granulated blast furnace slag. Their results showed that the multivariate polynomial regression model accurately predicted the compressive strength with an error rate of less than 10%. To construct a high-order polynomial surrogate model, Jinglai, et al. [58] proposed an incremental modeling approach that employs the zeros of Chebyshev polynomials. Their method uses a space-filling scheme to generate an initial set of samples and incrementally selects additional samples while updating the polynomial order. This approach has been applied to two engineering applications. In summary, multivariate polynomial regression is a powerful tool that can be used to accurately model complex relationships between multiple predictor variables and a response variable in various fields.

The stability of rotors supported by journal bearings is a critical consideration in many mechanical applications. Friswell, et al. [59] employed a univariate polynomial fitting approach to directly estimate critical speeds. The aforementioned approach involves determining the polynomial coefficients by minimizing the residual discrepancies between the bearing dynamic stiffness obtained through hydrodynamic theory or experimental procedures and the polynomial expression. Miraskari, et al. [35] conducted a study on the dynamics of flexible rotors mounted on two identical journal bearings. The loading conditions in their study allowed for symmetric force distributions in both bearings. The authors employed four different methods to obtain the rotor-bearing solution, including direct solution of Reynolds equation using finite difference, short bearing analysis, linear first-order bearing stiffness and damping coefficients, and second-order stiffness and damping bearing coefficients. Their results showed that below the threshold speed, the four methods produced well-matched results, which is

consistent with the findings of Sayed and El-Sayed [36]. El-Sayed and Sayed [38] studied the nonlinear dynamics and continuation analysis of flexible rotors based on third-order bearing stiffness and damping coefficients. They developed a method to allow the use of continuation analysis while using bearing coefficients.

The stability of the rotor-bearing model was analyzed by Smolík, et al. [60] using four different methods to evaluate the nonlinear hydrodynamic forces: the finite element method, finite difference method, infinitely short bearing, and an approximate solution derived by modifying the short bearing theory. Sayed and El-Sayed [61] employed the MATCONT toolbox to investigate the stability, bifurcation, and limit cycle continuation of rotor bearing systems. Anastasopoulos and Chasalevris [62] investigated the bifurcation analysis of rotor bearing systems with a more realistic geometry profile for the journal bearings. They used numerical continuation of the solution branches employing both MATCONT and AUTO-07P continuation codes.

Recent research in the field of journal bearings has explored various factors that affect their performance, including bearing misalignment, fluid turbulence, magnetorheological fluids, and surface irregularities. Feng et al. [63] conducted a study on water lubricated journal bearings, investigating both the static and dynamic behavior. They considered the impact of fluid turbulence, bearing thermohydrodynamics, and misalignment effects. Perturbation analysis was employed to evaluate the bearing coefficients in their study. Sahu et al.[64] focused on the influence of misalignment and surface irregularities in magnetorheological fluid journal bearings. They utilized the modified Reynolds equation to evaluate the bearing coefficients in their analysis. Xiang et al.[65] investigated the performance of water lubricated journal bearings under the coupling of fluid, solid, and thermal conditions. They proposed a method to enhance the wear resistance and improve the contact performance of the bearing. Their numerical results indicated that the profile modification method is strongly influenced by design parameters and operating conditions. Cai et al. [66] introduced a mathematical model for coupled thrust and journal bearings lubricated with low viscosity fluids. They developed a five-degree-of-freedom rotor model to describe the dynamic behavior of the coupled bearing system. They validated the steady-state response under different operating conditions using published experimental data. In the current research, our focus is solely on traditional bearings without complicating factors. This allows for the clear introduction of the present method that utilizes polynomial functions to represent the nonlinear bearing forces.

The precise and rapid evaluation of the nonlinear pressure distribution within journal bearings is essential, particularly for the dynamic analysis of mechanical systems incorporating such bearings. Numerous methodologies have been proposed to approximate the bearing forces; however, several of these methods exhibit noteworthy limitations. While certain approaches exhibit satisfactory approximation capabilities under both static and dynamic load conditions, others have solely been validated in static scenarios. Among the various techniques, the Database method emerges as one that yields favorable outcomes for dynamic analyses, as presented by Chasalevris et al. [50]. To this end, the present study aims to improve the database method by utilizing a multivariable regression to convert the database into a four-dimensional polynomial space [67]. The resulting four-dimensional polynomial functions can be seamlessly integrated into the equations of motion for dynamical systems. This facilitates the application of dynamical analysis tools such as Hopf bifurcation analysis and numerical continuation, thereby enabling a better understanding of the dynamical system. The evaluated functions are tested by investigating the nonlinear dynamics of a rotor supported in journal bearings. After this introduction, Section 2 provides a detailed outline of the methodology employed to solve the Reynolds equation. Following this, Section 3 presents the proposed dynamical model. The verification results are then presented in Section 4, followed by a comprehensive discussion of the proposed model in Section 5. Finally, Section 6 summarizes the key findings obtained from the analysis and presents the concluding remarks.

2. Analysis of Finite Length Journal Bearing

The forces generated by rotor dynamics are transmitted from the rotor to the structure via the bearings. In the case of journal bearings, the pressure distribution of the fluid film between the rotor and the bearings is influenced by both the rotational speed and the applied forces. The evaluation of bearing forces involves integrating the pressure distribution in the fluid film over the surface. The equation that describes the pressure distribution in journal bearings is known as Reynolds equation, which is shown in Eq. (1). Figure 1 depicts the schematic for a full circular journal bearing model, where O_B, O_J, and e represent the bearing and journal centers and eccentricity between them, respectively. The dynamic bearing forces are obtained by utilizing a full circular journal bearing model. R and r are the bearing and journal radii, and the radial clearance between the journal and bearing is c. ϕ and θ represent the circumference coordinate and the journal bearing angle of attitude respectively. Ω denotes the rotational velocity of the journal, while h signifies the thickness of the

oil film.

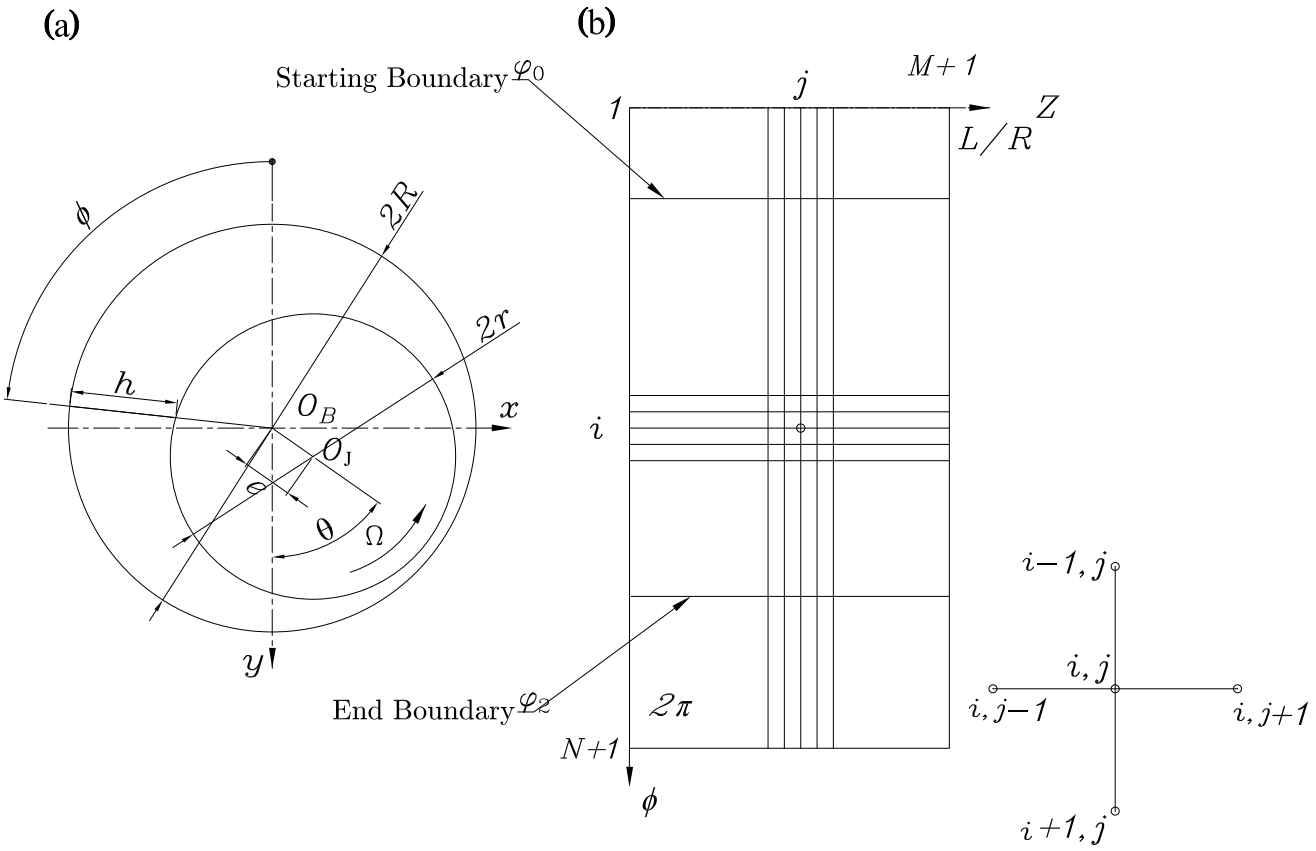

Figure 1: Full circular journal bearing model (a) Coordinates of the journal bearing (b) mesh of journal bearing.

The fluid film Reynolds equation Eq. (1) describes the pressure distribution in the fluid film between a rotating journal and its surrounding bearing. The fluid is assumed to be incompressible, isoviscous, and Newtonian.

$$\frac{1}{r^2}\frac{\partial}{\partial\phi}\left(\frac{\rho h^3}{12\mu}\frac{\partial p}{\partial\phi}\right)+\frac{\partial}{\partial z}\left(\frac{\rho h^3}{12\mu}\frac{\partial p}{\partial z}\right)=\frac{\Omega}{2}\frac{\partial(\rho h)}{\partial\phi}+\rho\frac{\partial h}{\partial t}, \tag{1}$$

where the symbols $p,\ \mu,\ \rho$ denote the pressure function, viscosity, and density, respectively, while z and t represent the axial coordinate and time, respectively.

The dimensionless form of Eq. (1) is expressed as follows,

$$\frac{\partial}{\partial\phi}\left(H^3\frac{\partial P}{\partial\phi}\right)+\frac{\partial}{\partial Z}\left(H^3\frac{\partial P}{\partial Z}\right)=\frac{\partial H}{\partial\phi}+2\frac{\partial H}{\partial\tau}, \tag{2}$$

where H represents the dimensionless oil-film thickness, P represents the dimensionless pressure, Z represents the dimensionless axial location, and τ represents the dimensionless time. These variables are related to the original physical variables as follows:

$H = \frac{h}{c}, \quad P = \frac{p}{6\mu\Omega}\left(\frac{c}{R}\right)^2, \quad Z = \frac{z}{R}$ and $\tau = \Omega$t .

Assuming no misalignment in the journal bearing, the oil-film thickness in dimensionless form H can be defined as

$$H = 1 + \varepsilon\cos(\phi - \theta) = 1 + X\sin\phi + Y\cos\phi, \tag{3}$$

where the dimensionless displacements of the journal center with respect to the bearing housing are denoted as $X = \frac{x}{c}$, $Y = \frac{y}{c}$. The derivatives of the oil film thickness with respect to the circumferential coordinate ϕ and the dimensionless time τ can be expressed as follows,

$$\frac{\partial H}{\partial \phi} = X\cos\phi - Y\sin\phi, \tag{4}$$

$$\frac{\partial H}{\partial \tau} = X'\sin\phi + Y'\cos\phi. \tag{5}$$

The Reynolds equation can be written by substituting Eqs. (4) and (5) into Eq. (2) as follows:

$$\frac{\partial}{\partial\phi}\left(H^3\frac{\partial P}{\partial\phi}\right) + \frac{\partial}{\partial Z}\left(H^3\frac{\partial P}{\partial Z}\right) = (X + 2Y')\cos\phi + (2X' - Y)\sin\phi. \tag{6}$$

Equation (6) reveals that the pressure distribution is dependent on the position of the journal center, represented by X and Y, as well as its velocity, denoted as (X', Y'). While the dimensionless journal center positions X and Y are theoretically bounded to a range between -1 and 1, the velocity components X' and Y' are unrestricted and can take values between $-\infty$ and ∞. However, to construct a comprehensive database for bearing forces, defining velocity subdivisions for X' and Y' is not feasible because their maximum values are undefined. In order to address this issue, Eq. (6) is divided by the magnitude of the right-hand side of Eq. (6), given by $\sqrt{(X + 2Y')^2 + (2X' - Y)^2}$. By doing so, Eq. (6) can be expressed as:

$$\frac{\partial}{\partial\phi}\left(H^3\frac{\partial P_n}{\partial\phi}\right) + \frac{\partial}{\partial Z}\left(H^3\frac{\partial P_n}{\partial Z}\right) = A_3\cos\phi + A_4\sin\phi. \tag{7}$$

and

$$
\begin{aligned}
P_n &= \frac{P}{\sqrt{(X+2Y')^2+(2X'-Y)^2}} \\
A_1 &= X, \\
A_2 &= Y, \\
A_3 &= \frac{X+2Y'}{\sqrt{(X+2Y')^2+(2X'-Y)^2}}, \\
A_4 &= \frac{2X'-Y}{\sqrt{(X+2Y')^2+(2X'-Y)^2}},
\end{aligned}
\tag{8}
$$

The finite difference method (FDM) is utilized to numerically solve Eq. (7) by discretizing the bearing surface into $M \times N$ elements, as depicted in Figure 1-b. At this point it should be noted that the Reynolds boundary conditions are considered. In Eq. (7), P_n depends on , $A_1 = X$, $A_2 = Y$, A_3, and A_4, all of which fall within the interval $[-1, 1]$. From Equation (8), it is evident that there exists a relationship between A_3 and A_4, which can be expressed as follows:

$$A_4 = \pm(1 - A_3^2)^{0.5} \tag{9}$$

The nonlinear bearing force terms F_{n_X} and F_{n_Y} can be calculated by integrating the pressure distribution function P_n over the journal bearing surface as follows:

$$F_{n_X} = \int_0^{\frac{L}{R}} \int_{\phi_0}^{\phi_2} -P_n \sin\phi \, \mathrm{d}\phi \, \mathrm{d}Z, \tag{10}$$

$$F_{n_Y} = \int_0^{\frac{L}{R}} \int_{\phi_0}^{\phi_2} -P_n \cos\phi \, \mathrm{d}\phi \, \mathrm{d}Z, \tag{11}$$

where ϕ_0 and ϕ_2 are the integration limits as shown in Fig. 1(b).

A discretized four-dimensional (4D) database is constructed utilizing the finite difference method (FDM) to solve Equation (7) and evaluate the bearing force terms F_{n_X} and F_{n_Y}. The construction of the database involves the discretization of the eccentricity ratio range, denoted as $\varepsilon \in [0 : 0.85]$, into 43 points with a step size of 0.02. Additionally, the bearing center angle, represented by $\theta \in [0 : 2\pi]$, is discretized into 40 points. Moreover, the parameter $A_3 \in [-1 : 1]$ is divided into 21 points. For each value of A_3, the corresponding two values of A_4 are obtained using Equation (9). This procedure yields a total of $43 \times 40 \times 21 \times 2 = 72{,}240$ data points within the database. The parameters $A_1 = X$

and $A_2 = Y$ can be determined through coordinate transformation, employing the variables ε and θ.

A multivariable polynomial regression is used to fit an equation to the present database. Then, the force components can be expressed in the following form:

$$\begin{aligned} F_{n_{X_\wp}}(A_1,\ A_2,\ A_3,\ A_4) =& \beta_0 + \sum_{j_1=1}^{4} \beta_{j_1} A_{j_1} + \sum_{j_1=1}^{4} \sum_{j_2=j_1}^{4} \beta_{j_1 j_2} A_{j_1} A_{j_2} + \\ & \ldots + \sum_{j_1=1}^{4} \sum_{j_2=j_1}^{4} \cdots \sum_{j_\wp=j_{\wp-1}}^{4} \beta_{j_1 j_2 \cdots j_\wp} A_{j_1} A_{j_2} \cdots A_{j_\wp} \end{aligned} \tag{12}$$

$$\begin{aligned} F_{n_{Y_\wp}}(A_1,\ A_2,\ A_3,\ A_4) =& \beta_0 + \sum_{j_1=1}^{4} \beta_{j_1} A_{j_1} + \sum_{j_1=1}^{4} \sum_{j_2=j_1}^{4} \beta_{j_1 j_2} A_{j_1} A_{j_2} + \\ & \ldots + \sum_{j_1=1}^{4} \sum_{j_2=j_1}^{4} \cdots \sum_{j_\wp=j_{\wp-1}}^{4} \beta_{j_1 j_2 \cdots j_\wp} A_{j_1} A_{j_2} \cdots A_{j_\wp} \end{aligned} \tag{13}$$

where, $\wp$ represents the highest polynomial order. The polynomial constants β of Eqs.(12) and (13) depend on the supplied data.

Assuming that $A_{i1},\ A_{i2},\ A_{i3},\ A_{i4}$ are the inputs for the database test points i, and z_i is the corresponding response, the obtained data can be written as

$$z_i = F_{n_X}(A_{i1},\ A_{i2},\ A_{i3},\ A_{i4}) + \varepsilon_i, \qquad i = 1, \cdots,\ N, \tag{14}$$

where the notation ε_i represents the uncertainty in evaluating a given point. In order to present the current data in matrix form as $\mathbf{A}$ which can be presented as follows

$$\mathbf{A}(i,:) = (1, A_{i1},\ A_{i2},\ A_{i3},\ A_{i4}; A_{i1}^2, A_{i1}A_{i2}, \cdots, A_{i4}^2; \cdots; A_{i1}^{\wp}, A_{i1}^{\wp-1}A_{i2}, \cdots, A_{i4}^{\wp}) \tag{15}$$

where the number of rows in $\mathbf{A}$ matrix is N and the corresponding $\boldsymbol{\beta}$ vector can be written as

$$\boldsymbol{\beta}^{\mathsf{T}} = (\beta_0, \beta_1,\ \beta_2,\ \beta_3,\ \beta_4; \beta_{11}, \beta_{12}, \cdots, \beta_{44}; \cdots; \beta_{1_{[\wp]}}, \beta_{1_{[\wp-1]}2}, \cdots, \beta_{4_{[\wp]}}), \tag{16}$$

where the subscript $\beta_{1_{[\wp]}}$ at $\wp = 3$ refers to β_{111} and $\beta_{4_{[\wp]}}$ at $\wp = 5$ indicates β_{44444}. It is worth mentioning that the semicolons used in Eqs. (15) and (16) are merely for organizational purposes and do not have any mathematical significance.

The proposed approach employs a matrix equation that establishes a relationship between the previously calculated data points and the corresponding estimated points obtained through a polynomial function,

$$\mathbf{z} = \mathbf{A}\boldsymbol{\beta} + \boldsymbol{\varepsilon}, \tag{17}$$

the vector $\mathbf{z}$ denotes the force data values for different inputs, presented in the form of a matrix $\mathbf{A}$.

The least square method is utilized to obtain a particular vector $\mathbf{b}$ of $\boldsymbol{\beta}$ that minimizes the sum of squared deviations. This is achieved by minimizing the following equation:

$$\sum_{i=1}^{N}[z_i - F_{n_X}(A_{i1},\ A_{i2},\ A_{i3},\ A_{i4})]^2 = (\mathbf{z} - \mathbf{A}\boldsymbol{\beta})^{\mathsf{T}}(\mathbf{z} - \mathbf{A}\boldsymbol{\beta}). \tag{18}$$

By differentiating the right-hand side of Equation (18) with respect to β and equating the result with zero, a vector $\mathbf{b}$ can be obtained as a sufficient condition using the following equation:

$$\mathbf{b} = (\mathbf{A}^{\mathsf{T}}\mathbf{A})^{-1}\mathbf{A}^{\mathsf{T}}\mathbf{z} \tag{19}$$

During the present work, multiple polynomial powers were tested to process the data and evaluate a 4D polynomial fit function. It was observed that degrees higher than 16 provide accurate results, as demonstrated in Section 4.3. However, it should be noted that the resulting polynomial equations can be quite large, and in this case, the size of the vector $\mathbf{b}$ is (4845×1), which translates to approximately tens of pages of written material.

The resulting 4D polynomial fit equation is utilized to evaluate the bearing forces as a function of the parameters $A_1,\ A_2,\ A_3$, and A_4. Specifically, the bearing forces in terms of the four-dimensional fit functions F_X and F_Y are evaluated as follows.

$$F_X = F_{n_X}\ \ \sqrt{(X + 2Y')^2 + (2X' - Y)^2}, \tag{20}$$

$$F_Y = F_{n_Y}\ \ \sqrt{(X + 2Y')^2 + (2X' - Y)^2}, \tag{21}$$

A flowchart outlining the algorithm used to obtain the journal bearing nonlinear forces is presented in Figure 2. In this study, the algorithm is referred to as the Four-Variable Polynomial Fit (FVP) method, and it involves fitting a four-dimensional polynomial function to the data obtained through the discretization of the bearing forces.

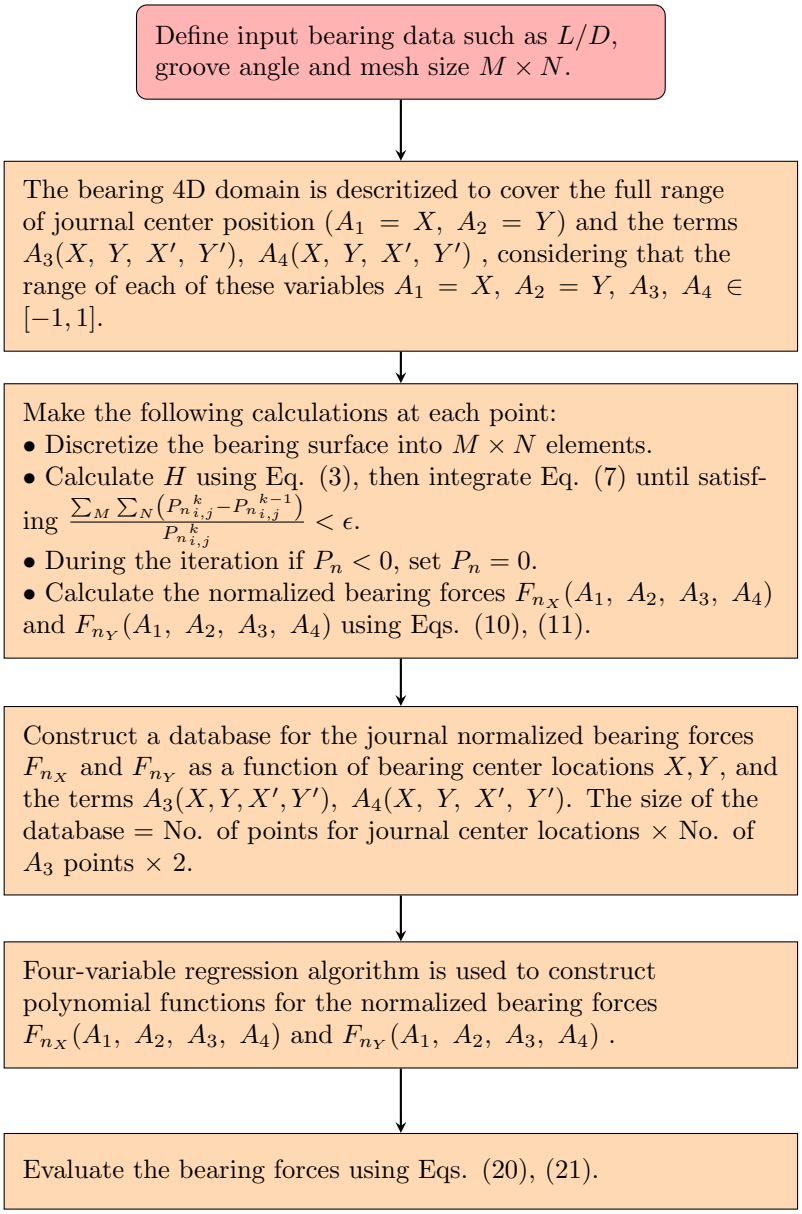

Figure 2: Flowchart outlining the steps used in the evaluation of the journal bearing nonlinear forces using the FVP method

3. The dynamical model of the example machine

This section examines the dynamic behavior of an elastic rotor supported on elastic bearing housings, as illustrated in Figure 3. The system comprises housing mass m_h, disc mass m_d, unbalanced mass of the disc m_u, and journal mass m_j. The total mass of the rotor is $m = m_d + 2m_j$. The housing and shaft stiffness constants are denoted by k_h and k_s, respectively. The unbalanced mass radius is represented by e_u, and c_h is the housing damping coefficient. The center of the journal is denoted as $o_j\,(x_j, y_j)$, while x_h and y_h are the housing displacements and x_d and y_d are the disc displacements. The journal bearing forces in Cartesian coordinates are F_x and F_y. The static load applied on the disc is $2W$, and unbalanced dynamic force is also considered. Gyroscopic effects are neglected in the

current model. The governing equations for the current rotor bearing model can be expressed as:

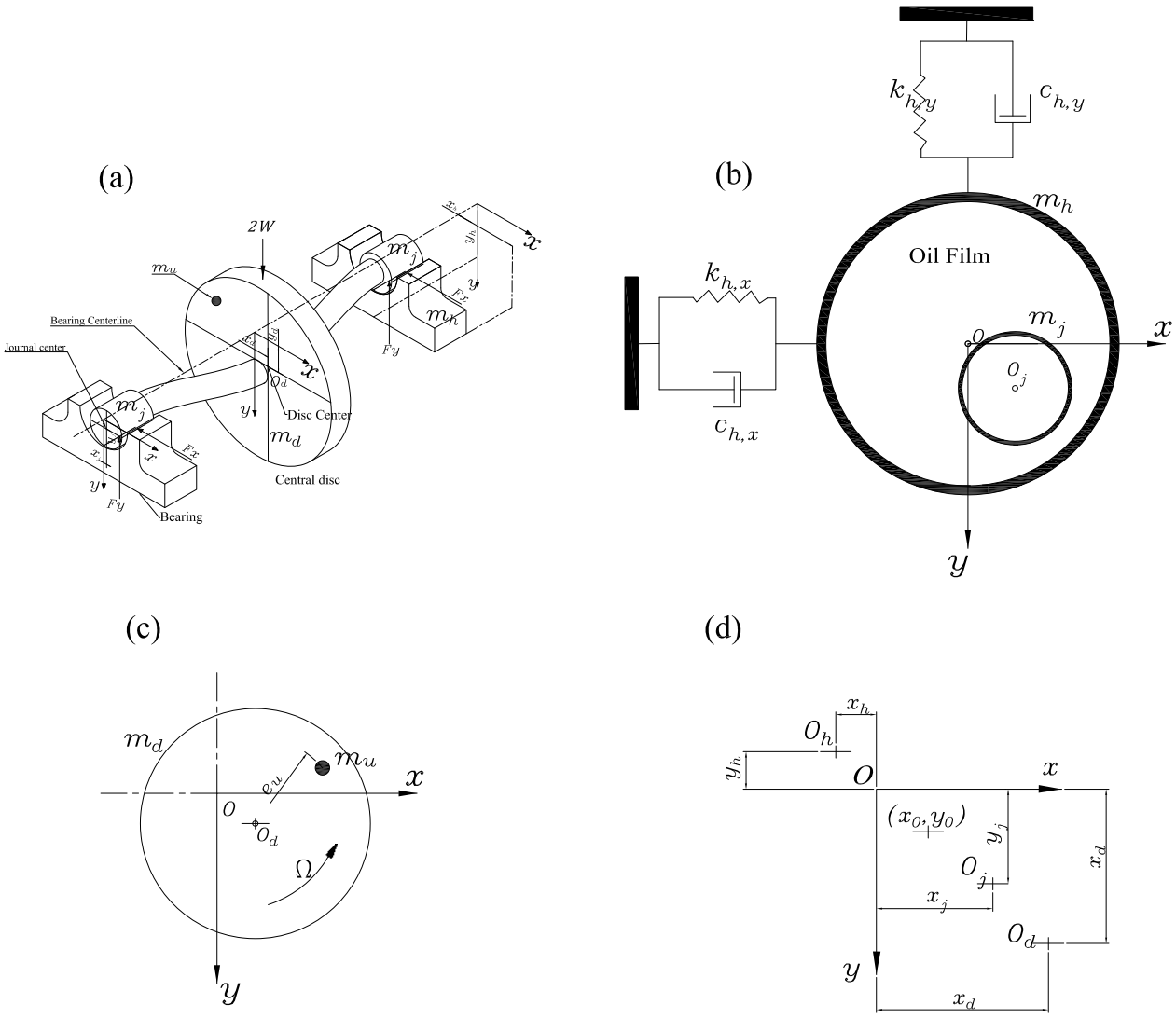

Figure 3: (a) Flexible rotor and disc model which is mounted on a couple of symmetrically loaded journal bearings. (b) Section view through the journal bearings. (c) Local view for the rotating disc. (d) representation for the coordinates used in the present Rotor-bearing system.

$$
\begin{aligned}
&2\ m_j\ \ddot{x}_j - k_s\ \ (x_d - x_j) + 2F_x = 0,\\
&2\ m_j\ \ddot{y}_j - k_s\ \ (y_d - y_j) + 2F_y = 0,\\
&m_d\ \ddot{x}_d + k_s\ \ (x_d - x_j) = -m_u e_u \Omega^2 \sin(\omega t),\\
&m_d \ddot{y}_d + k_s\ \ (y_d - y_j) = 2W - m_u e_u \Omega^2 \cos(\omega t),\\
&m_h \ddot{x}_h + c_h \dot{x}_h + k_h\ x_h = F_x,\\
&m_h\ \ddot{y}_h + c_h \dot{y}_h + k_h\ y_h = F_y.
\end{aligned}
\tag{22}
$$

Table 1: Dimensionless parameters for the machine example

Parameter	$\bar{M}_J$	$\bar{M}_D$	$\bar{M}_H$	$\bar{K}_H$	$\bar{C}_H$
	$0.1\ \bar{M}$	$0.8\bar{M}$	$\bar{M}$	100	2

The relatively simple rotor model in this study serves to emphasize the effectiveness of the proposed bearing model. However, it should be noted that the approach can be readily applied to more complex shaft models, such as those modeled using finite element analysis.

To facilitate analysis, the governing equations in Eq. (22) can be transformed into a dimensionless form using the following conversions: $X_I = \frac{x_i}{c},\ Y_I = \frac{y_i}{c},\ X_I' = \frac{\dot{x}_I}{\Omega c},\ Y_I' = \frac{\dot{y}_I}{\Omega c},\ X_I'' = \frac{\ddot{x}_I}{\Omega^2 c}\ ,\ Y_I'' = \frac{\ddot{y}_I}{\Omega^2 c},\ \bar{M}_I = \frac{m_i\ c\ \Omega^2}{W}$, where $i = \ h,\ \ j,\ \ d$ represents the housing, journal, and disc, respectively. The dimensionless stiffness constants are given by $\bar{K}_I = \frac{k_i\ c}{W}$, where $i = s,\ h$ for the shaft and housing, respectively. The dimensionless damping coefficient is denoted by $\bar{C}_H = \frac{c_h\ \Omega\ c}{W}$, and the dimensionless unbalance force is represented by $\bar{F}_u = \frac{m_u\ e_u\ \Omega^2}{W}$. The rotor dynamic equations can then be expressed in dimensionless form as follows:

$$
\begin{aligned}
&2\bar{M}_J X_J'' + \bar{K}_S\left(X_J - X_D\right) = -2\bar{F}_X,\\
&2\bar{M}_J Y_J'' + \bar{K}_S\left(Y_J - Y_D\right) = -2\bar{F}_Y,\\
&\bar{M}_D X_D'' + \bar{K}_S\left(X_D - X_J\right) = -\bar{F}_u \sin\left(\tau\right),\\
&\bar{M}_D Y_D'' + \bar{K}_S\left(Y_D - X_J\right) = 2 - \bar{F}_u \cos\left(\tau\right),\\
&\bar{M}_H X_H'' + \bar{C}_H X_H' + \bar{K}_H X_H = \bar{F}_X,\\
&\bar{M}_H Y_H'' + \bar{C}_H Y_H' + \bar{K}_H Y_H = \bar{F}_Y,
\end{aligned}
\tag{23}
$$

The dimensionless bearing forces in the x and y directions are defined as $\bar{F}_X = \frac{F_x}{W} = \frac{F_X}{\bar{W}}$ and $\bar{F}_Y = \frac{F_y}{W} = \frac{F_Y}{\bar{W}}$, respectively, where F_X and F_Y are computed using Eqs. (20) and (21), with $X = X_J - X_H$, $Y = Y_J - Y_H$, $X' = X_J' - X_H'$, and $Y' = Y_J' - Y_H'$. The load on the bearing and the dimensionless load are denoted by W and $\bar{W}$, respectively, with $\bar{W} = \frac{L/D}{3\pi\ S}$. The dimensionless mass of the rotor (disc and shaft) is defined as $\bar{M} = \frac{m\ c\ \Omega^2}{W} = \bar{M}_D + 2\bar{M}_J$. Table 1 shows the parameters utilized in this model.

Equation (23) can be written in vector form

$$
x' = f\left(x, \bar{M}\ \right), \tag{24}
$$

where the detailed equations are given by

$$
\begin{aligned}
x_1' &= x_2 \ , \\
x_2' &= -\frac{\bar{K}_S\left(x_1 - x_5\right)}{2\bar{M}_J} - \frac{\bar{F}_X}{\bar{M}_J}, \\
x_3' &= x_4 \ , \\
x_4' &= -\frac{\bar{K}_S\left(x_3 - x_7\right)}{2\bar{M}_J} - \frac{\bar{F}_Y}{\bar{M}_J} \quad , \\
x_5' &= x_6, \\
x_6' &= \frac{\bar{K}_S\left(x_1 - x_5\right) - \bar{F}_u \sin\left(\tau\right)}{\bar{M}_D}, \\
x_7' &= x_8, \\
x_8' &= \frac{2 + \bar{K}_S\left(x_3 - x_7\right) - \bar{F}_u \cos\left(\tau\right)}{\bar{M}_D}, \\
x_9' &= x_{10}, \\
x_{10}' &= \frac{\bar{F}_X - \bar{C}_H x_{10} - \bar{K}_H x_9}{\bar{M}_H}, \\
x_{11}' &= x_{12}, \\
x_{12}' &= \frac{\bar{F}_Y - \bar{C}_H x_{12} - \bar{K}_H x_{11}}{\bar{M}_H}.
\end{aligned}
\tag{25}
$$

where $\begin{bmatrix} x_1 & x_2 & x_3 & x_4 & x_5 & x_6 & x_7 & x_8 & x_9 & x_{10} & x_{11} & x_{12} \end{bmatrix} =$
$\begin{bmatrix} X_J & X_J' & Y_J & Y_J' & X_D & X_D' & Y_D & Y_D' & X_H & X_H' & Y_H & Y_H' \end{bmatrix}$.

4. Model validation

This section aims to validate the model and present the corresponding results. The model validation includes comparisons with previous literature, an examination of the accuracy of the nonlinear bearing forces obtained using the FVP analysis, and an investigation of the optimal FVP polynomial degree to accurately predict the nonlinear bearing forces.

4.1. FVP results comparison with previous literature

In this section, we present a validation of the FVP method used to evaluate the pressure and forces by comparing our results with those of previous literature. The model validation is divided into four parts. Firstly, we compare our results with those of Qiu [68] and Lund and Thomsen [69] by selecting

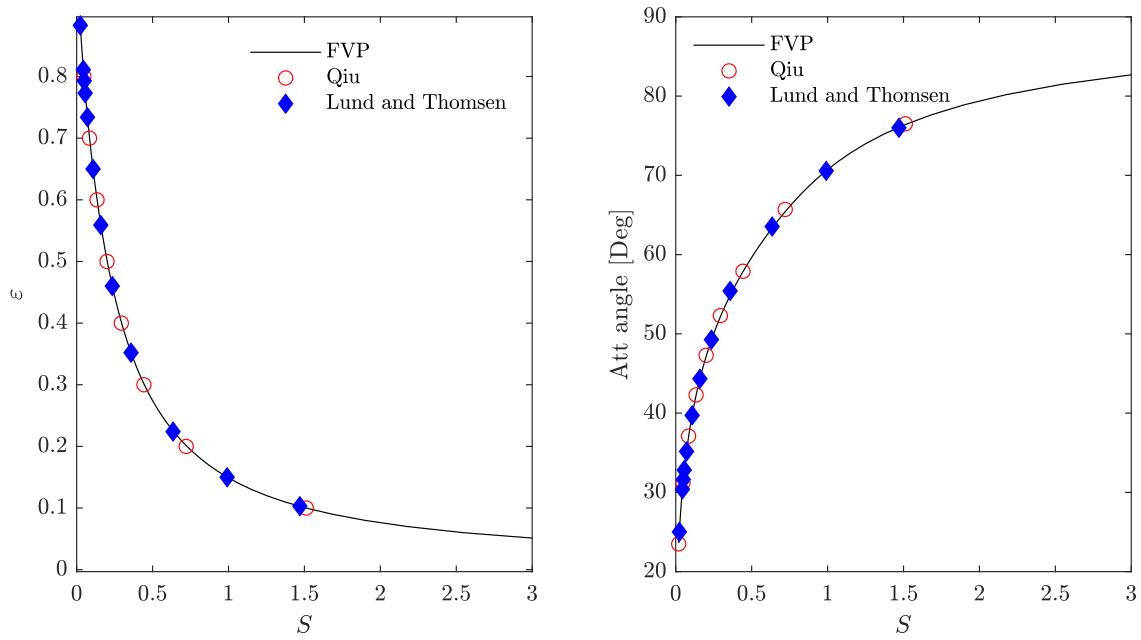

Figure 4: Comparison between the present FVP method in evaluating the equilibrium point with the work of both Qiu[68] and Lund and Thomsen [69], for 20° grooved journal bearing and slenderness ratio of 1.

the model parameters as ($\bar{K}_S = 10000,\ \bar{K}_H = 10000,\ \bar{C}_H = 0,\ \bar{M}_H = 0.001\bar{M},\ \bar{M}_J = 0.001\bar{M}$, and $\bar{M}$ is the selected small value $\bar{M} = 1$) to simulate a rigid rotor model. Additionally, FVP functions are prepared for 20° grooved journal bearing and slenderness ratio of 1. The dynamical model is allowed to run until reaching the equilibrium point at several values of the Sommerfeld number. The results are plotted against those of Qiu and Lund and Thomsen in Figure 4. Moreover, the equilibrium point can be obtained by equating $F_x = 0$ and $F_y = W$ at several Sommerfeld numbers without using the dynamic model.

Secondly, the present threshold dimesionless mass results are compared with those of Tieu and Qiu [70] and Lund [69] for 20° grooved journal bearing and slenderness ratio of 1 by selecting the model parameters to represent a rigid rotor model using ($\bar{K}_S = 10000,\ \bar{K}_H = 10000,\ \bar{C}_H = 0,\ \bar{M}_H = 0.001\ \bar{M},\ \bar{M}_J = 0.001\ \bar{M}$). It should be noted that the threshold dimensionless mass $\bar{M}_{th} = \frac{m\ c\ \Omega_{th}^2}{W}$ is corresponding to the threshold speed Ω_{th}. The threshold dimensionless mass obtained using the FVP analysis is compared with that of Lund and Thomsen [69] and Tieu and Qiu [70], and excellent matching results are obtained as shown in Figure 5.

Thirdly, the results obtained from the FVP analysis are used to recreate the trajectory of journal motion as presented by Tieu and Qiu [70]. This is accomplished by considering three dimensionless masses $\bar{M}$ of $2{\times}1.23^2$, $2{\times}2.69^2$, and $2{\times}3.28^2$, as depicted in Figure 6(a), (b) and (c) respectively. The first case is below the threshold speed, and the trajectory reaches the equilibrium point, while the

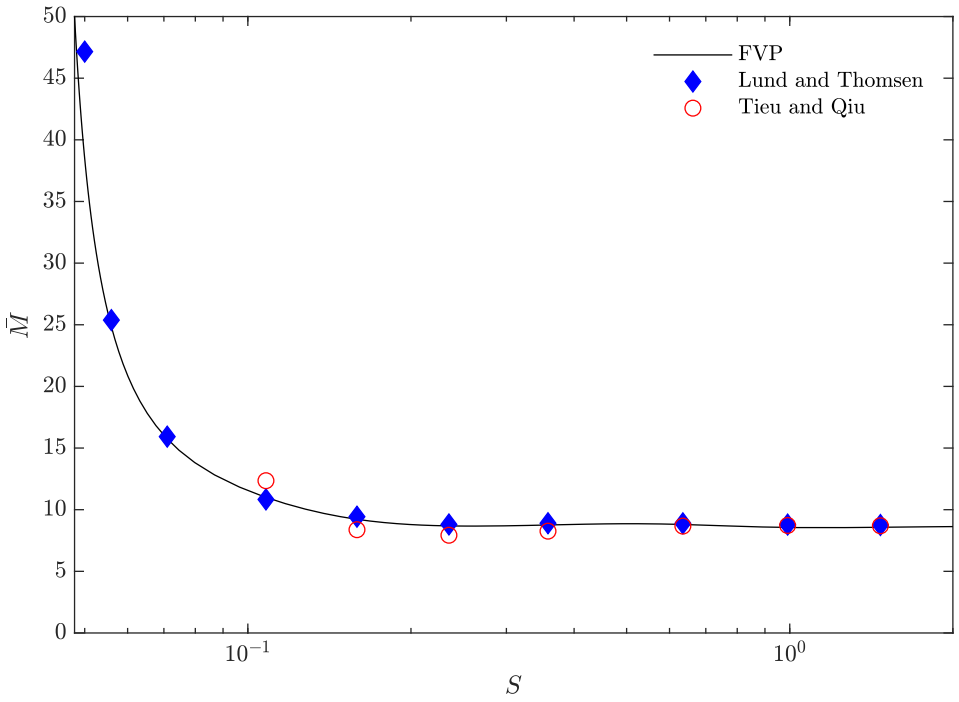

Figure 5: Comparison between the present FVP method in evaluating the threshold dimensionless mass with the work of Tieu and Qiu [70] Lund and Thomsen [69], for 20° grooved journal bearing and slenderness ratio of 1.

other two cases are above the threshold speed, and the rotor trajectory ends up in a limit cycle. The reference model parameters ($\bar{K}_S = 10000,\ \bar{K}_H = 10000,\ \bar{C}_H = 0;\ \bar{M}_H = 0.001\ \bar{M},\ \bar{M}_J = 0.001\ \bar{M}$); are used to represent the model, and the initial conditions of $X_J = X_D = X_H = Y_J = Y_D = Y_H = 0$ are set. The present rotor trajectories are in excellent agreement with those of Tieu and Qiu, as illustrated in Figure 6.

Finally, the obtained nonlinear polynomial force functions from the FVP equations (20-21) are utilized directly to determine the bearing stiffness and damping coefficients. The bearing coefficients

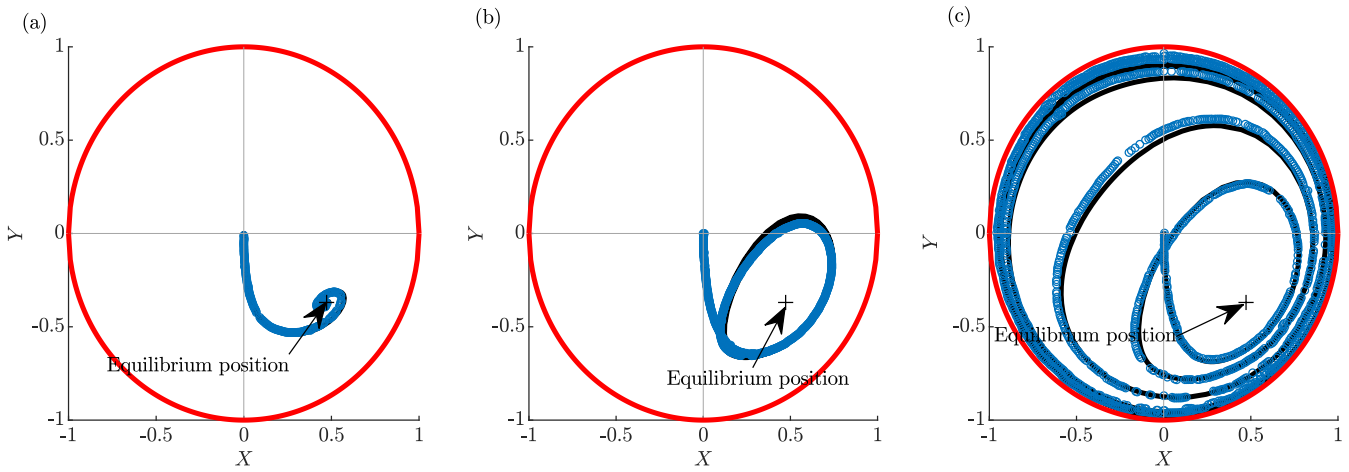

Figure 6: Rotor trajectory using the present FVP method to recreate the results of Tieu and Qiu [70], for ungrooved journal bearing and slenderness ratio of 1, at three different dimensionless mass $\bar{M}$ (a)2×1.23^2,(b) 2×2.69^2, (c)2×3.28^2

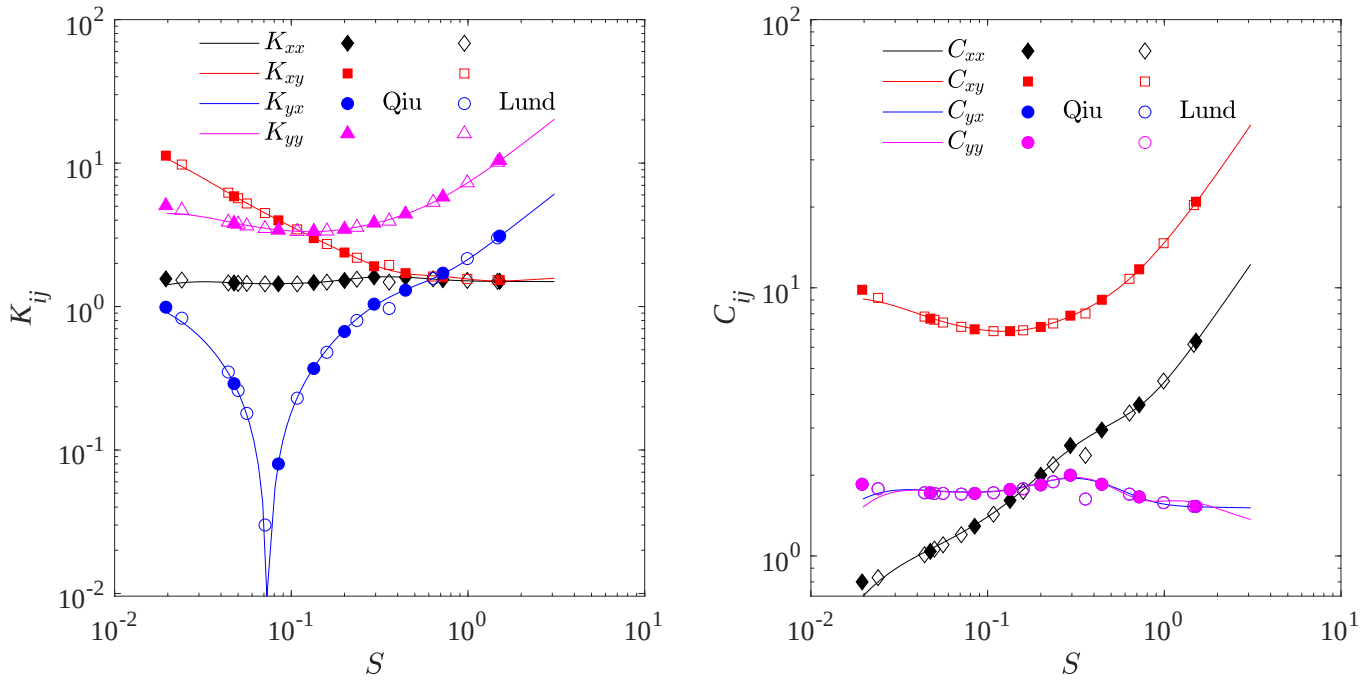

Figure 7: (color online) Variation of journal bearing stiffness and damping coefficients with Sommerfeld number. The solid lines depict the results obtained by differentiating equations (20-21), while the filled markers represent the findings of Qiu [68], and the unfilled markers correspond to the results of Lund and Thomson [69].

are calculated by differentiating the nonlinear forces of the bearing described in equations (20-21). Subsequently, these computed values are compared to the results obtained from the prior works of Qiu [68] and Lund and Thomson [69]. The comparison results are presented in Figure 7, which serves as an indicator of the accuracy achieved by the FVP polynomial function in determining the bearing stiffness and damping coefficients.

4.2. FVP results validation using perturbation analysis

In this section, the validity of the proposed approach is investigated by examining its ability to accurately evaluate nonlinear bearing forces resulting from perturbations in the rotor bearing system. Three cases of perturbations with increasing magnitudes are considered, and the resulting nonlinear forces are evaluated using three different approaches: integrating the Reynolds nonlinear equation (FRe), third order bearing coefficients (FC3), and four variable polynomial fitting (FVP).

At this particular point in the discussion, it is crucial to clarify that the process of determining perturbed forces using the Reynolds nonlinear equation (FRe) involves the application of perturbations, followed by the evaluation of the pressure distribution in the oil film based on the updated position. This pressure is then integrated over the bearing area to obtain the updated force due to the perturbation. In contrast, evaluating the bearing force using third order bearing coefficients (FC3)

necessitates the use of infinitesimal perturbations to initially calculate the bearing's first, second, and third order coefficients in the vicinity of the equilibrium point. Once the bearing coefficients have been determined, they can be used to calculate the force resulting from any perturbation from the equilibrium point. For further elaboration, please refer to [38].

The magnitudes of the perturbations applied in the considered cases are as follows: case I involves small perturbations, with magnitudes of $\delta X = \delta Y = 0.01$ and $\delta X' = \delta Y' = 0.01$. In case II, the perturbations are of larger magnitude, with $\delta X = \delta Y = 0.1$ and $\delta X' = \delta Y' = 0.01$. Finally, case III involves the largest perturbations among the considered cases, with magnitudes of $\delta X = \delta Y = 0.1$ and $\delta X' = \delta Y' = 0.2$. The x and y force components are obtained for each approach, and the results are plotted in Figure 8 over the possible range of Sommerfeld numbers.

For small perturbations (case I), the three methods yield similar results in evaluating the bearing force components. However, as the perturbation values increase in cases II and III (shown in the second and third rows of Figure 8), the FVP results closely match the FRe solution. In contrast, the FC3 approach shows significant differences in the evaluated forces compared to both the FVP and FRe methods for cases II and III.

The results also indicate a slight deviation between the FVP and FRe solutions at small values of Sommerfeld number less than 0.1. In conclusion, the proposed FVP method is found to be accurate in evaluating the bearing nonlinear forces even for large perturbations, and may be considered as a suitable replacement to the FRe method.

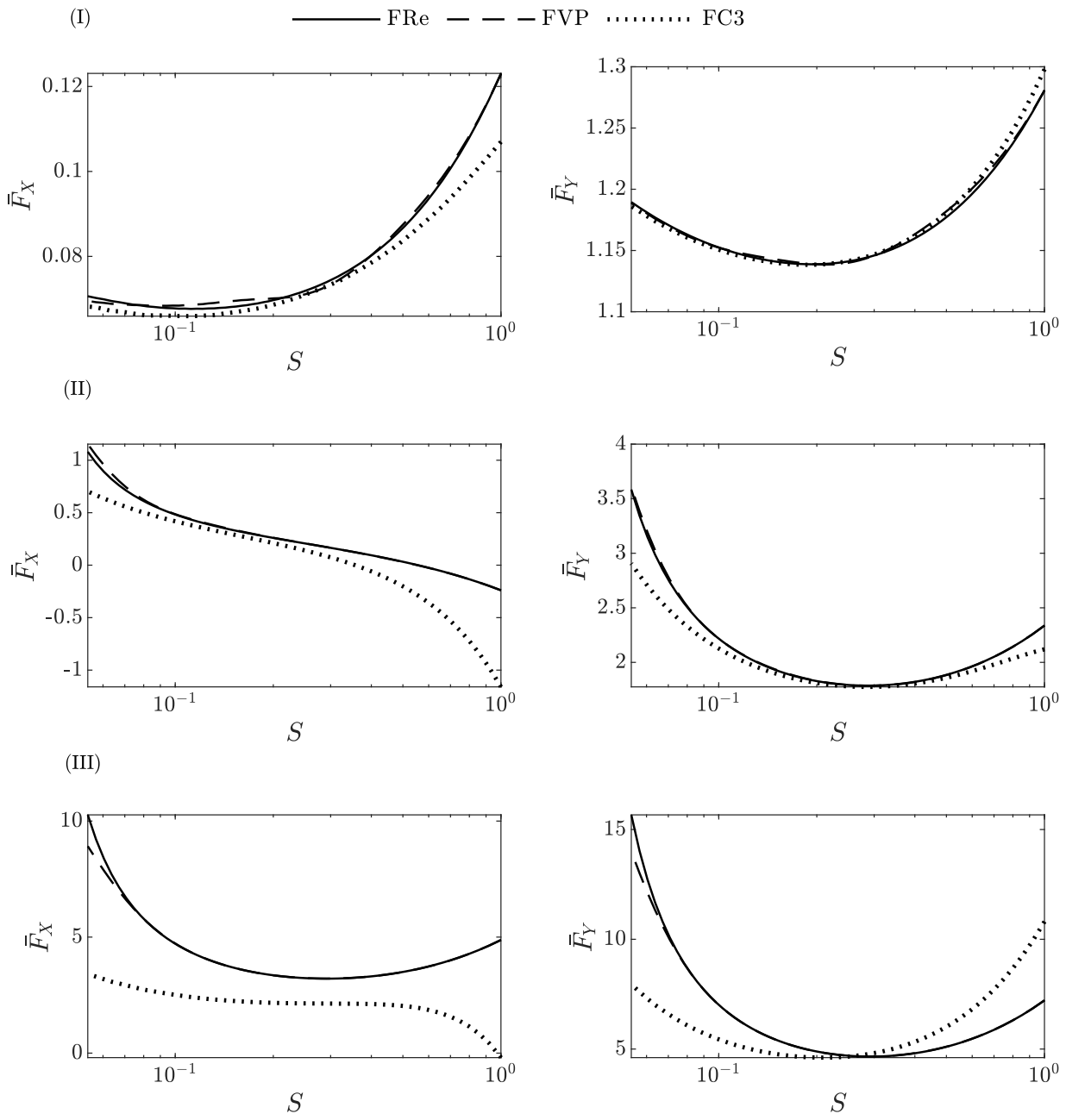

Figure 8: Components of perturbed nonlinear bearing forces $\bar{F}_X$, $\bar{F}_Y$ from the equilibrium position versus Sommerfeld number. The forces are evaluated using the direct solution of Reynolds equation (solid line), the proposed FVP method (dashed line) and the third order bearing coefficient FC3 method (dotted line). The perturbation values are I (top row): ($\delta X = \delta Y = 0.01,\ \delta X' = \delta Y' = 0.01$), II (middle row): ($\delta X = \delta Y = 0.1,\ \delta X' = \delta Y' = 0.01$) and III (bottom row): ($\delta X = \delta Y = 0.1, \delta X' = \delta Y' = 0.2$)

4.3. Effect of the order of multivariate polynomial

This section investigates the efficacy of multivariate polynomial fitting functions in estimating nonlinear bearing forces. To this end, the bearing forces resulting from three distinct perturbations are evaluated using the FRe method and compared with the forces obtained from the corresponding FVP functions. Five different polynomial function powers of order 8, 12, 16, 18 and 20 are employed for the FVP functions, as illustrated in Fig. 9. Furthermore, three different perturba-

tions, labeled (I)($\delta X = \delta Y = 0.01, \delta X' = \delta Y' = 0.01$) , (II)($\delta X = \delta Y = 0.1, \delta X' = \delta Y' = 0.01$), and (III)($\delta X = \delta Y = 0.1, \delta X' = \delta Y' = 0.2$), are utilized for the comparison, with varying magnitudes of perturbation.

Our findings indicate that, in all investigated cases, the multivariate polynomial fitting function of order 16 and higher yields accurate estimates of nonlinear forces in comparison with the force results from solving Reynolds equation. Therefore, we adopt the use of the multivariate polynomial of power 16 to estimate bearing forces in the subsequent analyses of this work.

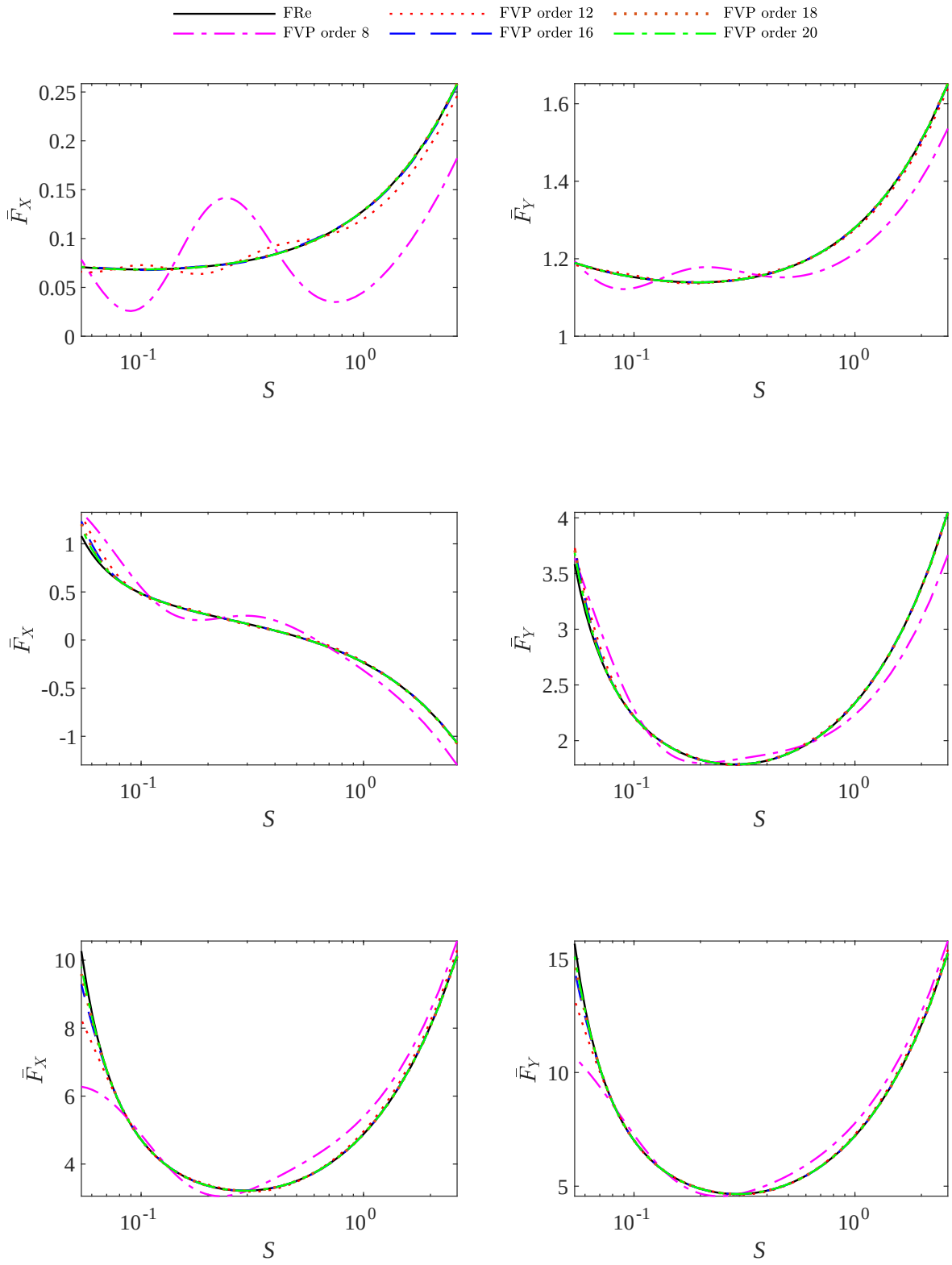

Figure 9: (color online) Effect of polynomial orders on the estimated polynomials forces resulted from a perturbations of (I)($\delta X = \delta Y = 0.01, \delta X' = \delta Y' = 0.01$), (II)($\delta X = \delta Y = 0.1, \delta X' = \delta Y' = 0.01$), (III) ($\delta X = \delta Y = 0.1, \delta X' = \delta Y' = 0.2$).

4.4. Effect of database density

Increasing the density of the database generally leads to an increase in fitting accuracy. However, this also results in an increase in the time required to build the database as well as the memory and time required for the regression analysis to construct the polynomial fitting function. In this section, we investigate the effect of database density on multivariate polynomial regression by utilizing three different densities, namely $(43 \times 40 \times 21 \times 2)$, $(22 \times 20 \times 21 \times 2)$, and $(22 \times 20 \times 11 \times 2)$, to evaluate the polynomial function. The obtained functions from the different databases are used in perturbation analysis to compare with the results obtained directly from the Reynolds function. Figure 10 illustrates the accuracy of the obtained functions in evaluating bearing forces for three different perturbation ranges, namely small perturbation (I) ($\delta X = \delta Y = 0.01, \delta X' = \delta Y' = 0.01$) to large perturbation (III) ($\delta X = \delta Y = 0.1, \delta X' = \delta Y' = 0.2$).

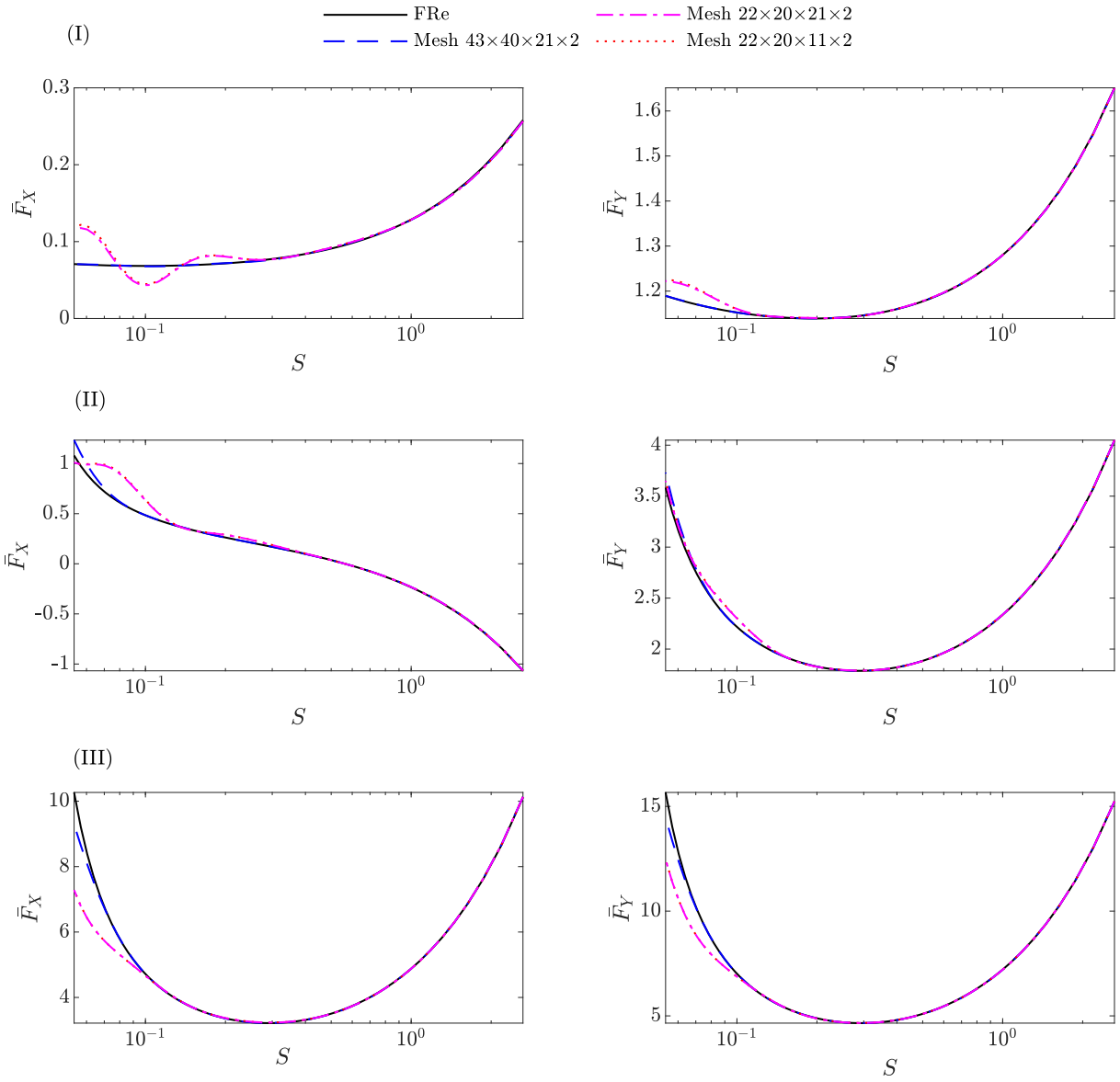

Figure 10: (color online) Effect of database density on the estimated polynomials forces resulted from a perturbations of (I)($\delta X = \delta Y = 0.01, \delta X' = \delta Y' = 0.01$), (II)($\delta X = \delta Y = 0.1, \delta X' = \delta Y' = 0.01$), (III) ($\delta X = \delta Y = 0.1, \delta X' = \delta Y' = 0.2$).

The findings depicted in the figure demonstrate the significant impact of database density on the resulting polynomial function. As can be observed from the figure, the function derived from the sparser mesh density of $(22 \times 20 \times 11 \times 2)$ yields the worst results. On the other hand, the function derived from mesh density $(22 \times 20 \times 21 \times 2)$ shows an improvement in the results compared to the sparser function. Notably, the results derived from the highest density mesh of $(43 \times 40 \times 21 \times 2)$ closely resemble those obtained from Reynolds equation. Therefore, it is worth mentioning that throughout the remainder of this paper, the database is constructed based on a mesh density of $(43 \times 40 \times 21 \times 2)$.

5. Present Model results

This section utilizes the FVP-derived forces to determine the threshold speed of the example rotor bearing model. Continuation analysis is then performed to investigate the dynamics of the rotor bearing model and the bifurcations that arise from changes in system parameters. Several time response cases are presented to verify the model results, and the effect of unbalanced forces is analyzed.

5.1. Analysis of the stability of the rotor bearing system

This section aims to analyze the stability of the rotor bearing system by obtaining the dimensionless threshold speeds. To achieve this, an ungrooved journal bearing with a slenderness ratio of 1 is used in the analysis. The dimensionless threshold speeds are determined for various rotor dimensionless stiffness values, namely $\bar{K}_S \in [0.5,\ 1,\ 2,\ 4,\ 8,\ 16,\ 10000]$, using the MATCONT toolbox. This toolbox, which is coded using the MATLAB interface, allows the coding and analyzing of Eq. (25).

The analysis begins by selecting an operating condition corresponding to a specific Sommerfeld number S. A small dimensionless mass $\bar{M}$ is then chosen to lie below the Hopf bifurcation conditions, and the dynamic equations are solved using Runge-Kutta direct numerical integration until an equilibrium point is reached. Then one parameter continuation in $\bar{M}$ is used to reach the Hopf bifurcation point, which is also known as the threshold speed. The type of bifurcation can be determined based on the sign of the largest Lyapunov exponent at this point, which can be either a supercritical or a subcritical Hopf bifurcation.

Next, a two-parameter continuation $(\bar{M},\ S)$ is utilized to evaluate the threshold speed line, as shown in Figure 11-a. This process is repeated for several values of the rotor dimensionless stiffness $\bar{K}_s$, which are plotted in Figure 11-a using different colors to represent each stiffness case. The solid segments in each line represent supercritical bifurcations, while the dashed segments indicate subcritical bifurcations. The results show a clear increase in the threshold speed as the rotor stiffness increases.

To evaluate the accuracy of the FVP method in determining the threshold speed, we consider the rotor dimensionless stiffness $\bar{K}_s = 8$ and compare the results obtained using both FVP and FRe methods. The results, as depicted in Figure 11-b, affirm that the proposed FVP method is accurate in determining the threshold speed.

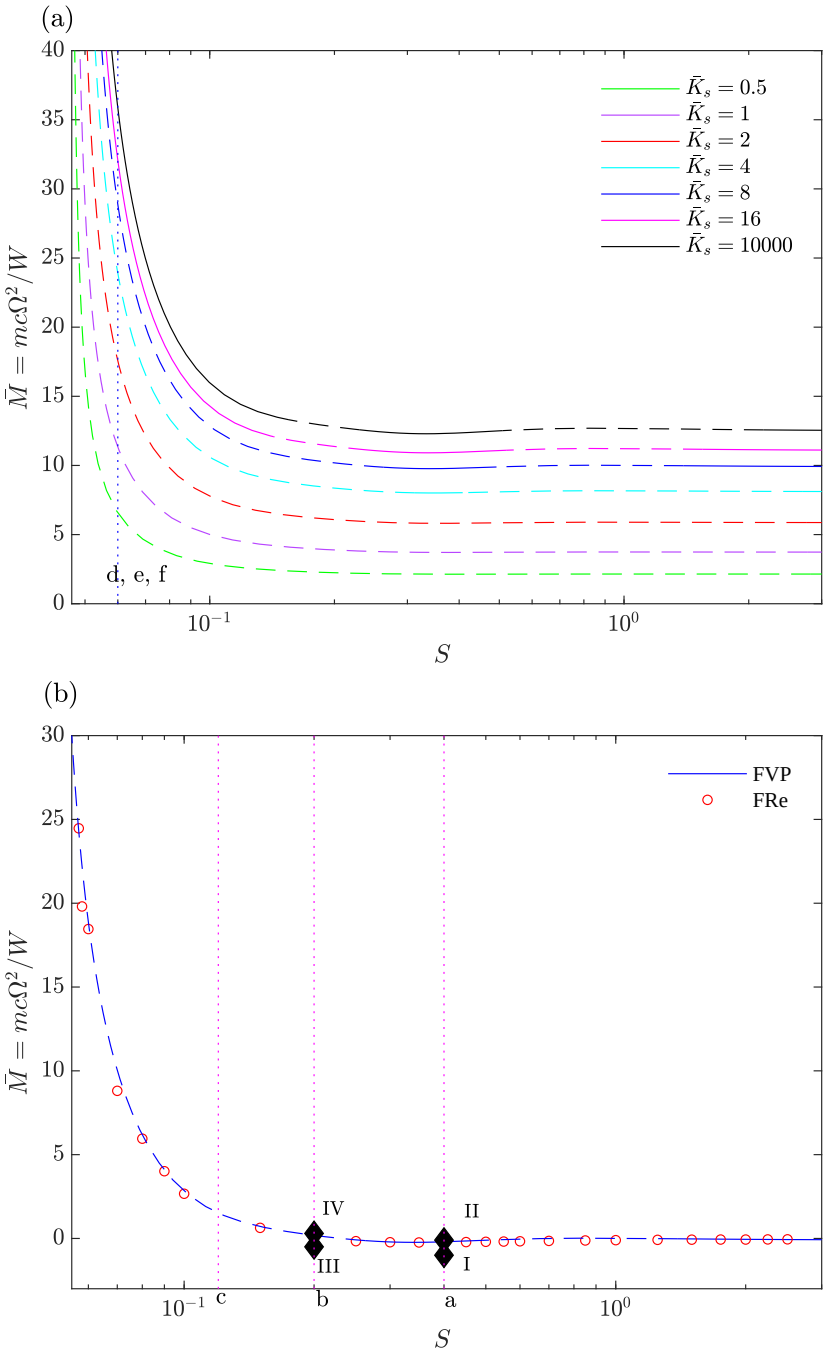

Figure 11: (color online) (a) Bearing threshold speed at several shaft stiffnesses. (b) Bearing threshold speed at shaft stiffness ratio of $\bar{K}_s = 8$ using both the FRe and proposed FVP methods. (Solid lines denote supercritical Hopf bifurcations and dash lines denote subcritical Hopf bifurcations).

5.2. Continuation analysis of limit cycles using FVP

Here, the continuation of limit cycles beyond the Hopf bifurcation point is investigated. Specifically, three loading conditions are considered : (a) ($\bar{K}_S = 8, S = 0.4$), (b) ($\bar{K}_S = 8, S = 0.2$), and (c) ($\bar{K}_S = 8, S = 0.12$). These cases are represented by the three vertically dotted lines in Figure 11-b. Figure 12 shows the continuation analyses for these cases where the first row provides a three-

dimensional representation of the limit cycle continuation. In the second row, a cross-section of the limit cycle plot is displayed, while the third row presents an orthogonal plan projection of the limit cycle continuation.

From Figure 11-b, it can be observed case (a) represents supercritical Hopf bifurcation, whereas cases (b) and (c) correspond to a subcritical Hopf bifurcation. For case (a), the supercritical Hopf bifurcation occurs at $\bar{M} = 9.8$. Further increase of $\bar{M}$ results in stable limit cycles growing until reaching a cycle known as limit point cycle at $\bar{M} = 9.974$. At this limit point cycle, the status of the limit cycle changes from stable to unstable and vice versa. Then, at $\bar{M} = 9.954$, another limit point cycle occurs, which is followed by stable limit cycles. For case (b), the subcritical Hopf bifurcation occurs at $\bar{M} = 10.185$. This is followed by a limit point cycle at $\bar{M} = 9.9$ where the unstable limit cycle becomes a stable limit cycle. Finally, for case (c), the subcritical Hopf bifurcation occurs at $\bar{M} = 11.514$. This is followed by another limit point cycles at $\bar{M} = 9.963$. Then, the system presents a stable limit cycle, as shown in the last column of Figure 12.

Figure 13 shows the limit cycle continuation for three cases having the same loading condition $S = 0.06$ in Figure 11-a and these cases are recorded as (d), (e) and (f). For these cases three different dimensionless shaft stiffnesses are used (d) $\bar{K}_S = 8$, (e) $\bar{K}_S = 16$, (f) $\bar{K}_S = 10000$. From Figure 11-a, it can be inferred that case (d) has a subcritical Hopf bifurcation while cases (e) and (f) have supercritical Hopf bifurcations. From Figure 11-a, it can be realized that increasing the shaft rigidity results in an increased $\bar{M}$ at the Hopf bifurcation point, as can be seen for cases (d, e and f) where the corresponding critical dimensionless mass equals $\bar{M} = (28.87,\ 32.062,\ 35.86)$ respectively.

For the flexible rotor case (d), a limit cycle point is observed at $\bar{M} = 10.197$. In cases (e) and (f), which are supercritical Hopf bifurcations, two limit cycle points are observed. The first limit cycle point occurs at $\bar{M} = 37.216$ and 67.56 for cases (e) and (f), respectively, followed by a second limit cycle point at $\bar{M} = 13.334$ and 17.87 for cases (e) and (f), respectively. It is important to note that each limit cycle point is accompanied by a transition from a stable/unstable limit cycle to an unstable/stable limit cycle, respectively. These results demonstrate the impact of rotor stiffness on the stability of the rotor-bearing system.

5.2.1. Rotor bearing response neglecting unbalance force

To further investigate the accuracy and effectiveness of the presented FVP method in obtaining nonlinear dynamics forces in the bearing, a trajectory plot for the current rotor-bearing system is

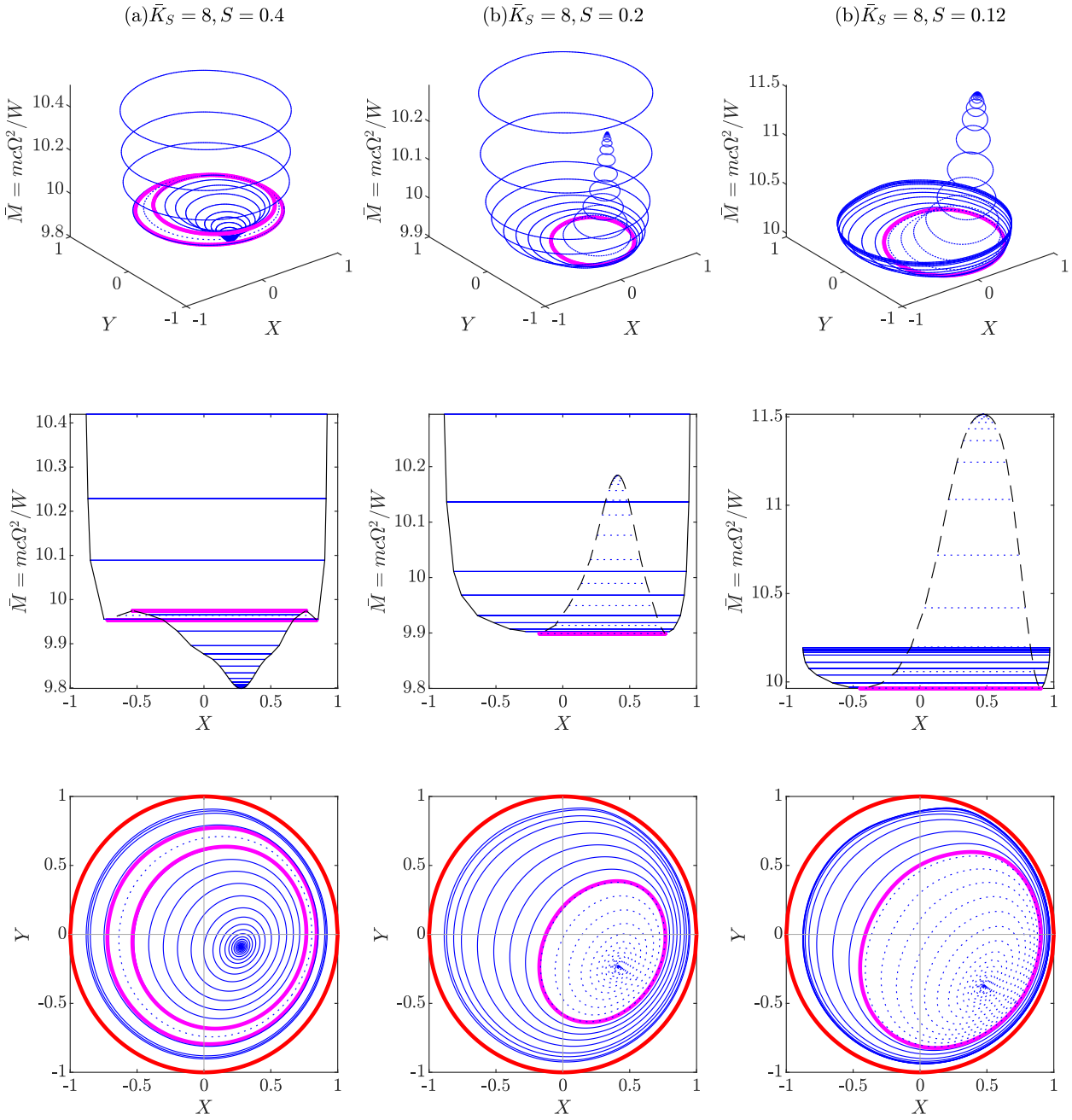

Figure 12: (color online) Rotor axis trajectory limit cycle continuation beyond the Hopf bifurcation. Three loading cases are considered: (a) $\bar{K}_S = 8, S = 0.4$ (b) $\bar{K}_S = 8, S = 0.2$ (c) $\bar{K}_S = 8, S = 0.12$. Solid lines indicate stable limit cycles, while dotted lines indicate unstable limit cycles.

analyzed using three different methods: FVP, FRe, and FC3 approaches [38]. The FRe approach is solved with a mesh size of 30×180. Four different cases are considered, denoted as I, II, III, and IV, as shown in Figure 11-b. The orbit plots for these cases are presented in Figure 14, where the first row (I) corresponds to $(\bar{K}_S = 8, S = 0.4, \bar{M} = 9)$, the second row (II) corresponds to $(\bar{K}_S = 8, S = 0.4, \bar{M} = 9.9)$, the third row (III) corresponds to $(\bar{K}_S = 8, S = 0.2, \bar{M} = 9.5)$, and the fourth row (IV) corresponds to $(\bar{K}_S = 8, S = 0.2, \bar{M} = 10.3)$. The first two rows show supercritical

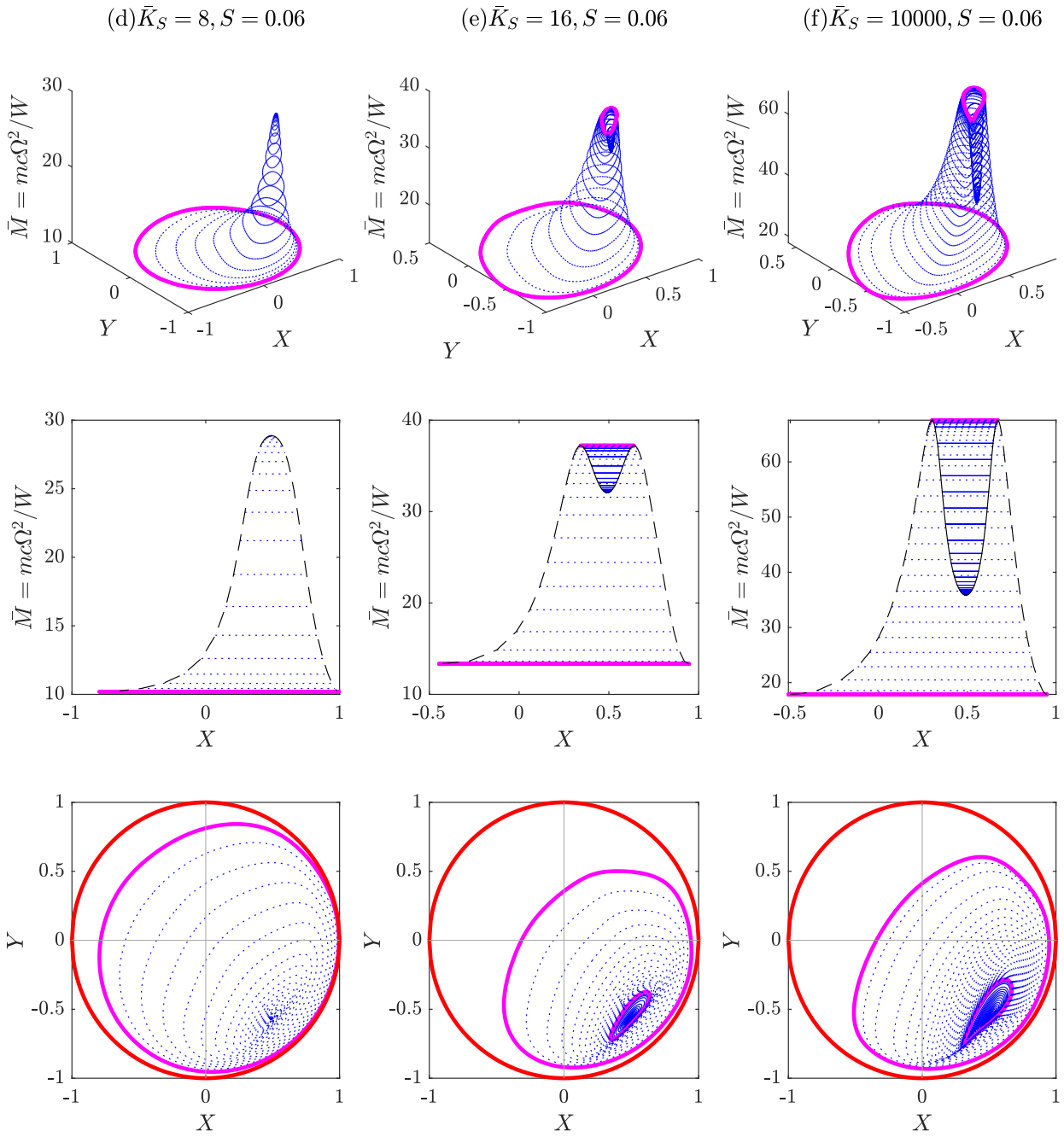

Figure 13: (color online) Rotor axis trajectory limit cycle continuation beyond the Hopf bifurcation. Three loading cases are considered at (d) $\bar{K}_S = 8, S = 0.06$ (e) $\bar{K}_S = 16, S = 0.06$ (f) $\bar{K}_S = 10000, S = 0.06$. Solid lines are used to represent stable limit cycle and dotted lines are used to represent the unstable ones.

conditions with the same Sommerfeld number, where the first row results are just below the Hopf bifurcation condition, and the second row results are just above the Hopf bifurcation condition. The last two rows of Figure 14 have the same Sommerfeld number and show subcritical conditions. The third row is just below the Hopf bifurcation, and the last row is above the Hopf bifurcation.

Figure 14 shows that for cases I and III, which are both below the Hopf bifurcation, the system responses obtained using the three methods are consistent. However, for case II, which is supercritical

Table 2: Computational time required for solving the cases I, II, III and IV which are shown in Figure 8

Case	S	$\bar{M}$	τ	Computational time (S)		
				FVP	FRe	FC3
I	0.4	9	500	12.21	445.492	0.171
II	0.4	9.9	2500	90.666	2510.652	0.368
III	0.2	9.5	800	20.948	663.16	0.283
IV	0.2	10.3	1700	83.429	4701.24	0.247

and above the Hopf bifurcation limit, the trajectory plot shows a small deviation between the response based on the FRe method and both the proposed FVP and FC3 methods.

Case IV represents an operating condition above the Hopf bifurcation and it is subcritical, for which the response evaluated using the FRe and FVP bearing forces are similar. However, the response based on the FC3 method is significantly different, as shown in the last row of Figure 14. These results suggest that the FVP method is an accurate and reliable approach to evaluate the nonlinear bearing forces in the rotor-bearing system.

Table 2 presents the computational time for the cases analyzed in Figure 14. The computational analysis was conducted on a computer system with an Intel(R) Core(TM) i7-6820HQ CPU, which has a clock speed of 2.70 GHz, and 16.0 GB of RAM. The computations were executed using MATLAB software in a single-core configuration. The results reveal that the fastest computational time is achieved by the solution based on evaluating bearing forces using the FC3 method. Nevertheless, the results demonstrate that there is a significant discrepancy in the simulated responses at speeds higher than the subcritical Hopf bifurcation when using the FC3 method. Moreover, the table indicates that the computational time for the FVP results is significantly shorter than that for the FRe solution. However, the computational time for the FVP method is longer than that for FC3. It can, therefore, be concluded that the proposed FVP method shows a significant reduction in computational time compared to the FRe method while maintaining computational accuracy.

5.3. Rotor bearing response considering unbalance force

Here, the effects of unbalance forces on the rotor-bearing system are investigated. The dimensionless stiffness of the shaft is set to $\bar{K}_S = 8$ and the Sommerfeld number is set to $S = 0.4$. The amplitude of the unbalance mass is set to $\bar{F}_u = 0.2\bar{M}_D$. The bifurcation diagram is analyzed over a dimensionless mass range of $\bar{M} = \frac{m\ c\ \omega^2}{W} \in [1, 13]$.

The bifurcation diagram results are plotted in Figure 15 and shows that period doubling occurs at $\bar{M} = 7.7$. With further increases in the dimensionless mass $\bar{M}$, a single limit cycle occurs at

$\bar{M} = 9.5$. Four cases are selected for further analysis, which are (a) $\bar{M} = 6$, (b) $\bar{M} = 8$, (c) $\bar{M} = 9$, and (d)$\bar{M} = 12$, identified by the four dotted lines in Figure 15. The orbit plots for these cases are then calculated using both the FRe and FVP methods, and the results are plotted in Figure 16. The first and second rows of Figure 16 correspond to the FVP and FRe analysis, respectively, and the bottom row shows the response FFT analysis. Each column in the figure represents one of the four cases (a, b, c, and d).

The results clearly demonstrate that the proposed FVP bearing forces analysis yields results similar to those obtained using the FRe solution. The FFT analysis for case (a) indicates a large amplitude at the frequency ratio of one (corresponding to the rotational speed of the rotor) and smaller amplitudes for superharmonic frequencies. Cases (b-d), which are above the critical dimensionless mass ($\bar{M} = 7.7$), exhibit high amplitudes at subharmonic frequencies (frequency ratio 0.5), high amplitude at the rotational speed of the rotor, and low amplitudes at superharmonic frequencies.

It is important to note that while the proposed method offers several advantages, it also has certain limitations. Specifically, the method requires a high number of data points in the four-dimensional space. Additionally, due to the significant increase in the fluid film stiffness near the clearance circle, the slope of the bearing forces in that region is very high. This presents a significant challenge when attempting to use a single polynomial function to represent the full bearing domain. In this study, a single polynomial function was utilized to cover the range of $\varepsilon \in [0 : 0.85]$. Moreover, it should be noted that the current analysis did not incorporate a cavitation model, which is an important factor and may affect the evaluation of bearing forces throughout the entire domain of the journal bearing.

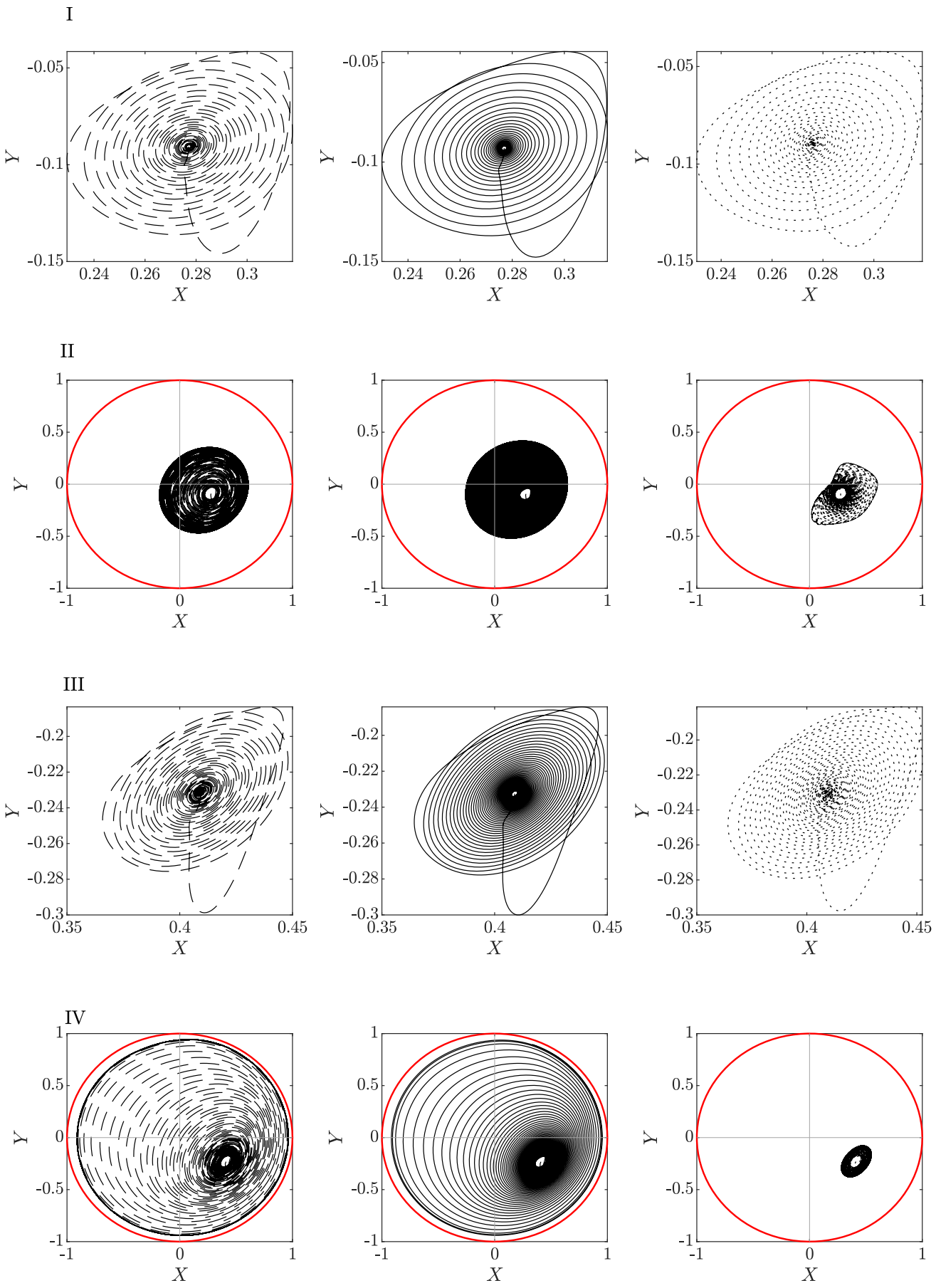

Figure 14: (color online) Orbit plots for the rotor used in the example dynamical model. The first column represents the FVP results, the middle column represents the FRe results and the last column represents the third order bearing coefficient results. The four rows represent four different operating conditions which are shown in Figure 11 b.

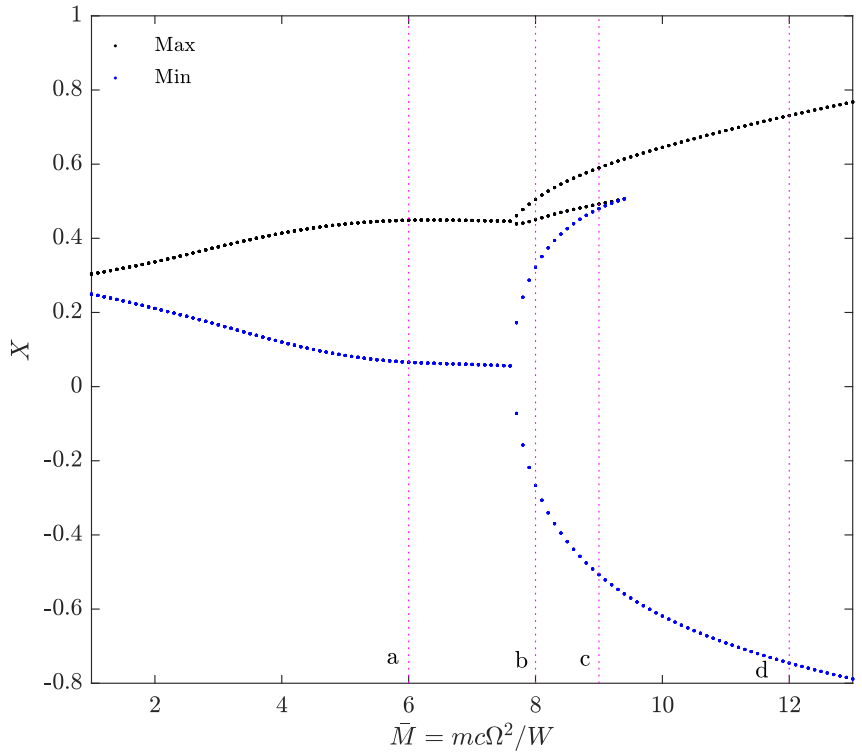

Figure 15: (color online) Bifurcation diagram for the rotor bearing system model. The vertical axis represents both the maximum and minimum $X = X_J - X_H$ displacement. The horizontal axis represents the nondimensional mass $\bar{M}$.

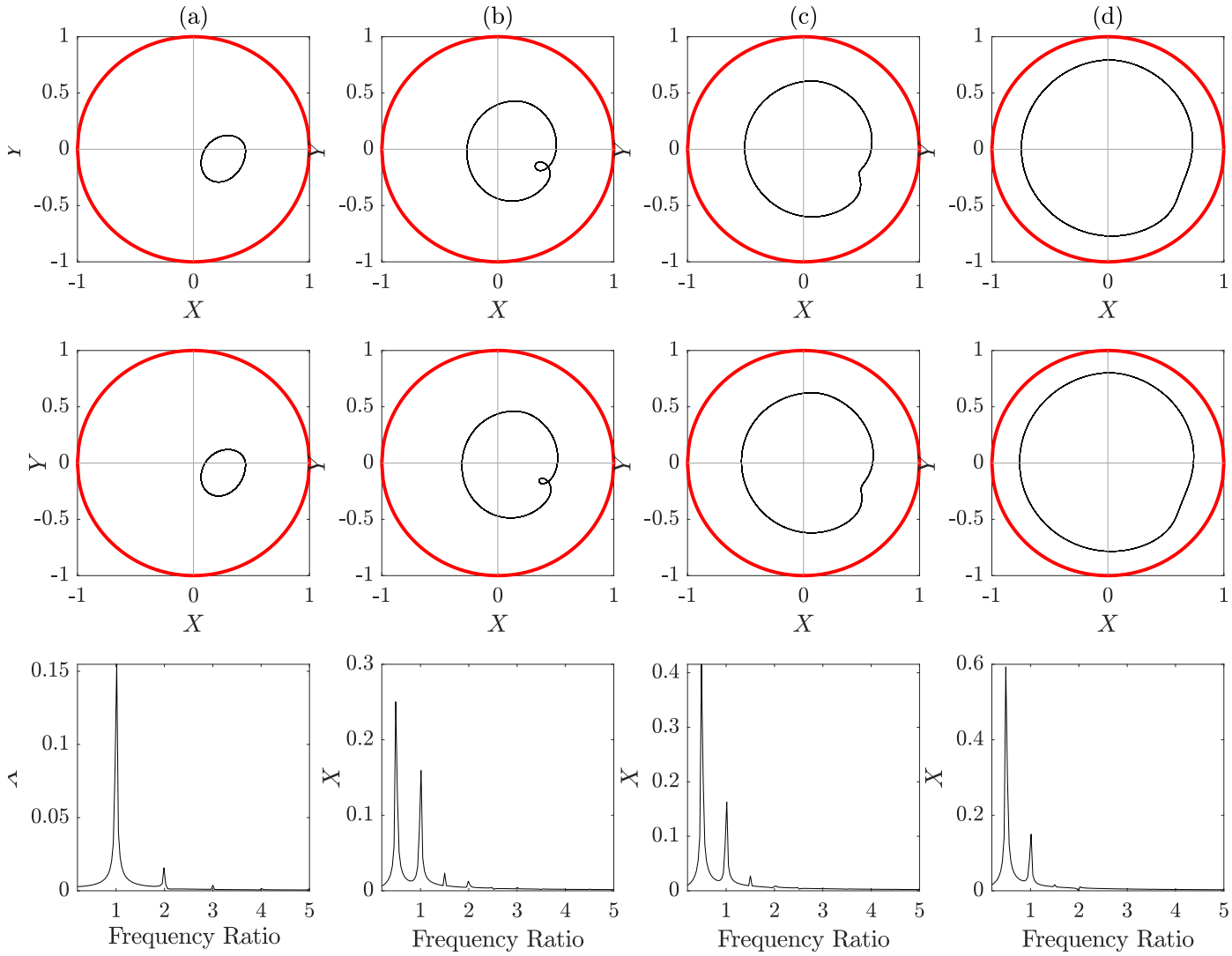

Figure 16: (color online) Orbit plots for cases a, b, c and d shown by dotted lines in Figure 15. These cases are shown in the four columns of this figure. The first row is obtained using the FVP solution and the second row is obtained using the FRe solution. The last row is the FFT for the four cases based on FVP.

Conclusions

This study proposes a novel method for the assessment of nonlinear forces arising from journal bearings. The proposed approach involves constructing a four-dimensional database for the bearing forces components in Cartesian coordinates, as a function of rotor center dimensionless displacement and velocity. Subsequently, a four-dimensional multivariable polynomial function is employed to approximate the nonlinear bearing force distribution.

The efficacy of the proposed method, termed FVP, is evaluated through a comparison with results from the literature. The results demonstrate that the FVP method yields a favorable agreement with literature values. Furthermore, the FVP method is compared with two other methods, namely the direct solution of the Reynolds equation (FRe) and the third-order bearing coefficient method (FC3), to assess system responses. The findings suggest that the bearing forces obtained through the FVP method are more accurate compared to those obtained via the FC3 method. Additionally, the computational time required for the FVP approach is found to be shorter than that of the FRe method, though longer than the FC3 method.

In conclusion, the FVP method offers an efficient and accurate approach for evaluating nonlinear forces in complex mechanical systems such as pumps and hydraulic turbochargers. This approach can be instrumental in the design and optimization of such systems.

Funding Information

The authors of this paper declare that the research conducted in this paper was not supported by any funding from external organizations.

Data availability statement

The datasets generated during and/or analyzed during the current study are available from the corresponding author on reasonable request.

Conflict of interest

The authors of this paper declare that they do not have any conflict of interest.

Acknowledgement

References

[1] R. Tiwari, Rotor systems: analysis and identification, CRC press, 2017.

[2] T. A. El-Sayed, A. A. Abdel Fatah, Performance of hydraulic turbocharger integrated with hydraulic energy management in SWRO desalination plants, Desalination 379 (2016) 85–92. doi:https://doi.org/10.1016/j.desal.2015.10.013.

[3] T. A. El-Sayed, S. H. Farghaly, Exact free vibration analysis of Timoshenko stepped shaft carrying elastically supported eccentric masses with application on SWRO mechanical system, Desalination 385 (2016) 194–206. doi:https://doi.org/10.1016/j.desal.2016.02.010.

[4] O. Reynolds, On the theory of lubrication and its application to Mr. Beauchamp tower's experiments, including an experimental determination of the viscosity of olive oil, Philosophical Transactions of the Royal Society of London 177 (1886) 157–234.
URL http://www.jstor.org/stable/109480

[5] D. Sfyris, A. Chasalevris, An exact analytical solution of the Reynolds equation for the finite journal bearing lubrication, Tribology International 55 (2012) 46–58.

[6] W. H. Liao, R. F. Lu, R. D. Chien, J. R. Lin, Linear stability analysis of long journal bearings: Couple stress fluid model, Industrial Lubrication and Tribology 57 (1) 21–27, cited By :7 DOI = 10.1108/00368790510575950, year = 2005, type = Journal Article.

[7] A. Amamou, M. Chouchane, Nonlinear stability analysis of long hydrodynamic journal bearings using numerical continuation, Mechanism and Machine Theory 72 (2014) 17–24. doi:https://doi.org/10.1016/j.mechmachtheory.2013.10.002.

[8] G. B. DuBois, F. W. Ocvirk, Analytical derivation and experimental evaluation of short-bearing approximation for full journal bearing, Report (1953).
URL https://digital.library.unt.edu/ark:/67531/metadc60530/

[9] F. W. Ocvirk, Short-bearing approximation for full journal bearings, Report, Citeseer (1952).
URL (https://digital.library.unt.edu/ark:/67531/metadc56460/

[10] A. Sommerfeld, The hydrodynamic theory of lubrication friction 50 (1-2) (1904) 97–155.

[11] H. Elrod, A. Burgdorfer, Refinement of the theory of the infinitely long self-acting gas lubricated journal bearing, Vol. 49, Office of Naval Research, Department of the Navy., 1960, p. 93.

[12] L. R. Gero, C. M. McC. Ettles, An evaluation of finite difference and finite element methods for the solution of the Reynolds equation, ASLE transactions 29 (2) (1986) 166–172.

[13] C. A. Heshmat, D. S. Xu, H. Heshmat, Analysis of gas lubricated foil thrust bearings using coupled finite element and finite difference methods, J. Trib. 122 (1) (2000) 199–204.

[14] C. M. Ettles, H. G. Anderson, The use of higher order finite element methods for the solution of Reynolds' equation, Tribology transactions 33 (2) (1990) 163–170.

[15] M. Arghir, A. Alsayed, D. Nicolas, The finite volume solution of the reynolds equation of lubrication with film discontinuities, International Journal of Mechanical Sciences 44 (10) (2002) 2119–2132. doi:https://doi.org/10.1016/S0020-7403(02)00166-2.

[16] A. W. Bush, Perturbation methods for engineers and scientists, Routledge, 2018.

[17] R. Nicoletti, Comparison between a meshless method and the finite difference method for solving the Reynolds equation in finite bearings, Journal of Tribology 135 (4) (2013).

[18] J. W. Lund, The stability of an elastic rotor in journal bearings with flexible, damped supports, Journal of Applied Mechanics 32 (4) (1965) 911–920. doi:https://doi.org/10.1115/1.3627335.

[19] J. W. Lund, Stability and damped critical speeds of a flexible rotor in fluid-film bearings, Journal of Engineering for Industry 96 (2) (1974) 509–517. doi:https://doi.org/10.1115/1.3438358.

[20] J.-P. Peng, M. Carpino, Calculation of stiffness and damping coefficients for elastically supported gas foil bearings, Journal of Tribology 115 (1) (1993) 20–27. doi:10.1115/1.2920982.

[21] v. Dyk, J. Rendl, M. Byrtus, L. Smolík, Dynamic coefficients and stability analysis of finite-length journal bearings considering approximate analytical solutions of the Reynolds equation, Tribology International 130 (2019) 229–244. doi:https://doi.org/10.1016/j.triboint.2018.09.011.

[22] Z. L. Qiu, A. K. Tieu, The effect of perturbation amplitudes on eight force coefficients of journal bearings, Tribology Transactions 39 (2) (1996) 469–475. doi:doi/abs/10.1080/10402009608983554.

[23] A. Chasalevris, D. Sfyris, Evaluation of the finite journal bearing characteristics, using the exact analytical solution of the Reynolds equation, Tribology International 57 (2013) 216–234. doi:https://doi.org/10.1016/j.triboint.2012.08.011.

[24] M. Miraskari, F. Hemmati, M. S. Gadala, Nonlinear Dynamics of Flexible Rotors Supported on Journal Bearings—Part I: Analytical Bearing Model, Journal of Tribology 140 (2) (2018). doi:https://doi.org/10.1115/1.4037730.

[25] Z. L. Qiu, A. K. Tieu, Misalignment effect on the static and dynamic characteristics of hydrodynamic journal bearings, Journal of Tribology (1995). doi:https://doi.org/10.1115/1.2831542.

[26] M. J. Goodwin, P. J. Ogrodnik, M. P. Roach, Y. Fang, Calculation and measurement of the stiffness and damping coefficients for a low impedance hydrodynamic bearing, Journal of Tribology (1997). doi:https://doi.org/10.1115/1.2832480.

[27] O. Ebrat, Z. P. Mourelatos, N. Vlahopoulos, K. Vaidyanathan, Calculation of journal bearing dynamic characteristics including journal misalignment and bearing structural deformation, Tribology Transactions 47 (1) (2004) 94–102. doi:https://doi.org/10.1080/05698190490278994. URL https://doi.org/10.1080/05698190490278994

[28] I. Arregui, C. Vázquez, Finite element solution of a Reynolds–Koiter coupled problem for the elastic journal–bearing, Computer Methods in Applied Mechanics and Engineering 190 (15-17) (2001) 2051–2062. doi:https://doi.org/10.1016/S0045-7825(00)00221-8.

[29] M. A. Hili, S. Bouaziz, M. Maatar, T. Fakhfakh, M. Haddar, Hydrodynamic and elastohydrodynamic studies of a cylindrical journal bearing, Journal of hydrodynamics 22 (2) (2010) 155–163. doi:https://doi.org/10.1016/S1001-6058(09)60041-X.

[30] G. Gao, Z. Yin, D. Jiang, X. Zhang, Y. Wang, Analysis on design parameters of water-lubricated journal bearings under hydrodynamic lubrication, Proceedings of the Institution of Mechanical Engineers, Part J: Journal of Engineering Tribology 230 (8) (2015) 1019–1029, doi: 10.1177/1350650115623201. doi:10.1177/1350650115623201.

[31] R. Tiwari, A. W. Lees, M. I. Friswell, Identification of dynamic bearing parameters: a review, Shock and Vibration Digest 36 (2) (2004) 99–124.

[32] T. Someya, J. Mitsui, J. Esaki, S. Saito, Y. Kanemitsu, T. Iwatsubo, M. Tanaka, S. Hisa, T. Fujikawa, H. Kanki, Journal-bearing databook, Springer Science & Business Media, 2013.

[33] A. Muszynska, Stability of whirl and whip in rotor/bearing systems, Journal of Sound and Vibration 127 (1) (1988) 49–64. doi:https://doi.org/10.1016/0022-460X(88)90349-5.

[34] J. C. Deepak, S. T. Noah, Experimental verification of subcritical whirl bifurcation of a rotor supported on a fluid film bearing, Journal of Tribology 120 (3) (1998) 605–609. doi:10.1115/1.2834593.

[35] M. Miraskari, F. Hemmati, M. S. Gadala, Nonlinear Dynamics of Flexible Rotors Supported on Journal Bearings—Part II: Numerical Bearing Model, Journal of Tribology 140 (2) (2018) 021705. doi:https://doi.org/10.1115/1.4037731.

[36] H. Sayed, T. A. El-Sayed, Nonlinear dynamics and bifurcation analysis of journal bearings based on second order stiffness and damping coefficients, International Journal of Non-Linear Mechanics 142 (2022) 103972. doi:https://doi.org/10.1016/j.ijnonlinmec.2022.103972.

[37] W. Weimin, Y. Lihua, W. Tiejun, Y. Lie, Nonlinear dynamic coefficients prediction of journal bearings using partial derivative method, Proceedings of the Institution of Mechanical Engineers, Part J: Journal of Engineering Tribology 226 (4) (2012) 328–339. doi:https://doi.org/10.1177/1350650111431526.

[38] T. A. El-Sayed, H. Sayed, Bifurcation analysis of rotor/bearing system using third-order journal bearing stiffness and damping coefficients, Nonlinear Dynamics 107 (1) (2022) 123–151. doi:10.1007/s11071-021-06965-4.

[39] E. K. Elsayed, H. Sayed, T. A. El-Sayed, Analysis of second-order thrust bearing coefficients considering misalignment effect, Journal of Vibration Engineering & Technologies (2023). doi:10.1007/s42417-023-00956-y.
URL https://doi.org/10.1007/s42417-023-00956-y

[40] J. V. Fedor, A sommerfeld solution for finite bearings with circumferential grooves, Journal of Basic Engineering 82 (2) (1960) 321–326. doi:10.1115/1.3662589.

[41] J. V. Fedor, Half Sommerfeld approximation for finite journal bearings, Journal of Basic Engineering 85 (3) (1963) 435–438. doi:10.1115/1.3656638.

[42] L. E. Barrett, P. E. Allaire, E. J. Gunter, A finite length bearing correction factor for short bearing theory, Journal of Lubrication Technology 102 (3) (1980) 283–287. doi:10.1115/1.3251508.
URL https://doi.org/10.1115/1.3251508

[43] H. Hirani, K. Athre, S. Biswas, Dynamically loaded finite length journal bearings: Analytical method of solution, Journal of Tribology 121 (4) (1999) 844–852. doi:10.1115/1.2834144.

[44] Y. Bastani, M. de Queiroz, A new analytic approximation for the hydrodynamic forces in finite-length journal bearings, Journal of Tribology 132 (1) (2009). doi:10.1115/1.4000389.
URL https://doi.org/10.1115/1.4000389

[45] Y. L. Wang, Z. S. Liu, W. J. Kang, J. J. Yan, Approximate analytical model for fluid film force of finite length plain journal bearing, Proceedings of the Institution of Mechanical Engineers, Part C: Journal of Mechanical Engineering Science 226 (5) (2011) 1345–1355, doi: 10.1177/0954406211418302. doi:10.1177/0954406211418302.

[46] Y. Zhang, X. Li, C. Dang, D. Hei, X. Wang, Y. Lü, A semianalytical approach to nonlinear fluid film forces of a hydrodynamic journal bearing with two axial grooves, Applied Mathematical Modelling 65 (2019) 318–332. doi:https://doi.org/10.1016/j.apm.2018.07.048.

[47] G. G. Vignolo, D. O. Barilá, L. M. Quinzani, Approximate analytical solution to Reynolds equation for finite length journal bearings, Tribology International 44 (10) (2011) 1089–1099. doi:https://doi.org/10.1016/j.triboint.2011.03.020.

[48] R.-Z. Gong, D.-Y. Li, H.-J. Wang, L. Han, D.-Q. Qin, Analytical solution of Reynolds equation under dynamic conditions, Proceedings of the Institution of Mechanical Engineers, Part J: Journal of Engineering Tribology 230 (4) (2015) 416–427, doi: 10.1177/1350650115604654. doi:10.1177/1350650115604654.

[49] Y. Zhang, D. Hei, C. Liu, B. Guo, Y. Lu, N. Müller, An approximate solution of oil film forces of turbulent finite length journal bearing, Tribology International 74 (2014) 110–120. doi:https://doi.org/10.1016/j.triboint.2014.02.015.

[50] A. Chasalevris, J.-C. Louis, Evaluation of transient response of turbochargers and turbines using database method for the nonlinear forces of journal bearings, Lubricants 7 (9) (2019) 78.
URL https://www.mdpi.com/2075-4442/7/9/78

[51] Z. Chen, Y. Jiao, S. Xia, W. Huang, Z. Zhang, An efficient calculation method of nonlinear fluid film forces in journal bearing, Tribology Transactions 45 (3) (2002) 324–329, doi: 10.1080/10402000208982556. doi:10.1080/10402000208982556.

[52] W. Wang, Z.-M. Zhang, X. Chen, Application of the non-stationary oil film force database, Journal of Shanghai University (English Edition) 5 (3) (2001) 230–233. doi:10.1007/s11741-996-0030-9.

[53] D. Kleinbaum, L. Kupper, A. Nizam, E. Rosenberg, Applied Regression Analysis and Other Multivariable Methods, Cengage Learning, 2013.
URL https://books.google.com.eg/books?id=v590AgAAQBAJ

[54] H. Gatignon, Statistical Analysis of Management Data, Springer New York, 2010.
URL https://books.google.com.eg/books?id=SyJhTpfvPwkC

[55] J. G. Lin, Modeling test responses by multivariable polynomials of higher degrees, SIAM Journal on Scientific Computing 28 (3) (2006) 832–867.

[56] J. Wei, T. Chen, G. Liu, J. Yang, Higher-order multivariable polynomial regression to estimate human affective states, Scientific reports 6 (1) (2016) 1–13.

[57] M. Su, Q. Zhong, H. Peng, Regularized multivariate polynomial regression analysis of the compressive strength of slag-metakaolin geopolymer pastes based on experimental data, Construction and Building Materials 303 (2021) 124529. doi:https://doi.org/10.1016/j.conbuildmat.2021.124529.
URL https://www.sciencedirect.com/science/article/pii/S0950061821022856

[58] J. Wu, Z. Luo, J. Zheng, C. Jiang, Incremental modeling of a new high-order polynomial surrogate model, Applied Mathematical Modelling 40 (7) (2016) 4681–4699. doi:https://doi.org/10.1016/j.apm.2015.12.002.
URL https://www.sciencedirect.com/science/article/pii/S0307904X15007945

[59] M. I. Friswell, S. D. Garvey, J. E. T. Penny, M. G. Smart, Computing critical speeds for rotating machines with speed dependent bearing properties, Journal of Sound and Vibration 213 (1) (1998) 139–158. doi:https://doi.org/10.1006/jsvi.1998.1503.
URL https://www.sciencedirect.com/science/article/pii/S0022460X98915036

[60] L. Smolík, J. Rendl, v. Dyk, P. Polach, M. Hajžman, Threshold stability curves for a nonlinear rotor-bearing system, Journal of Sound and Vibration 442 (2019) 698–713. doi:https://doi.org/10.1016/j.jsv.2018.10.042.

[61] H. Sayed, T. A. El-Sayed, A novel method to evaluate the journal bearing forces with application to flexible rotor model, Tribology International 173 (2022) 107593. doi:https://doi.org/10.1016/j.triboint.2022.107593.

[62] L. Anastasopoulos, A. Chasalevris, Bifurcations of limit cycles in rotating shafts mounted on partial arc and lemon bore journal bearings in elastic pedestals, Journal of Computational and Nonlinear Dynamics (2022). doi:https://doi.org/10.1115/1.4053593.

[63] H. Feng, S. Jiang, A. Ji, Investigations of the static and dynamic characteristics of water-lubricated hydrodynamic journal bearing considering turbulent, thermohydrodynamic and misaligned effects, Tribology International 130 (2019) 245–260. doi:https://doi.org/10.1016/j.triboint.2018.09.007.
URL https://www.sciencedirect.com/science/article/pii/S0301679X1830447X

[64] K. Sahu, S. C. Sharma, N. Ram, Misalignment and surface irregularities effect in mr fluid journal bearing, International Journal of Mechanical Sciences 221 (2022) 107196. doi:https://doi.org/10.1016/j.ijmecsci.2022.107196.
URL https://www.sciencedirect.com/science/article/pii/S0020740322001205

[65] G. Xiang, T. Yang, J. Guo, J. Wang, B. Liu, S. Chen, Optimization transient wear and contact performances of water-lubricated bearings under fluid-solid-thermal coupling condition using profile modification, Wear 502-503 (2022) 204379. doi:https://doi.org/10.1016/j.wear.2022.204379.
URL https://www.sciencedirect.com/science/article/pii/S0043164822001405

[66] J. Cai, G. Xiang, S. Li, J. Guo, J. Wang, S. Chen, T. Yang, Mathematical modeling for nonlinear dynamic mixed friction behaviors of novel coupled bearing lubricated with low-viscosity fluid, Physics of Fluids 34 (9) (2022) 093612. doi:10.1063/5.0108943.
URL https://doi.org/10.1063/5.0108943

[67] A. Cecen, Multivariate polynomial regression (2022).
URL (https://github.com/ahmetcecen/MultiPolyRegress-MatlabCentral),GitHub.RetrievedApril16,2022.

[68] Z. L. Qiu, A theoretical and experimental study on dynamic characteristics of journal bearings, Thesis (1995).
URL http://ro.uow.edu.au/theses/1567

[69] J. Lund, K. Thomsen, A calculation method and data for the dynamic coefficients of oil-lubricated journal bearings, in: Topics in fluid film bearing and rotor bearing system design and optimization, ASME, Chicago, IL, 1978, pp. 1–28.

[70] A. K. Tieu, Z. L. Qiu, Stability of finite journal bearings—from linear and nonlinear bearing forces, Tribology Transactions 38 (3) (1995) 627–635, doi: 10.1080/10402009508983452. doi:10.1080/10402009508983452.
URL https://doi.org/10.1080/10402009508983452